Supplemental material to this article can be found at:
http://molpharm.aspetjournals.org/content/suppl/2021/12/14/molpharm.121.000354.DC1
1521-0111/101/3/168–180$35.00
MOLECULAR PHARMACOLOGY
dx.doi.org/10.1124/molpharm.121.000354
Mol Pharmacol 101:168–180, March 2022

Senolytic-Mediated Elimination of Head and Neck Tumor Cells Induced Into Senescence by Cisplatin

Fereshteh Ahmadinejad,[1] Tasia Bos,[1] Bin Hu, Erin Britt, Jennifer Koblinski, Andrew J. Souers, Joel D. Leverson, Anthony C. Faber, David A. Gewirtz, and Hisashi Harada[S]

Department of Human and Molecular Genetics, School of Medicine (F.A.), Philips Institute for Oral Health Research, School of Dentistry (T.B., E.B., A.C.F., H.H.), Cancer Mouse Models Core (B.H., J.K.), and Department of Pharmacology and Toxicology, School of Medicine (D.A.G.), Massey Cancer Center, Virginia Commonwealth University, Richmond, Virginia; and AbbVie, North Chicago, Illinois (A.J.S., J.D.L.)

Received July 1, 2021; accepted November 25, 2021

ABSTRACT

Therapeutic outcomes achieved in head and neck squamous cell carcinoma (HNSCC) patients by concurrent cisplatin-based chemoradiotherapy initially reflect both tumor regression and tumor stasis. However, local and distant metastasis and disease relapse are common in HNSCC patients. In the current work, we demonstrate that cisplatin treatment induces senescence in both p53 wild-type HN30 and p53 mutant HN12 head and neck cancer models. We also show that tumor cells can escape from senescence both in vitro and in vivo. We further establish the effectiveness of the senolytic, ABT-263 (Navitoclax), in elimination of senescent tumor cells after cisplatin treatment. Navitoclax increased apoptosis by 3.3-fold ($P \leq 0.05$) at day 7 compared with monotherapy by cisplatin. Additionally, we show that ABT-263 interferes with the interaction between B-cell lymphoma-x large (BCL-X_L) and BAX, anti- and pro-apoptotic proteins, respectively, followed by BAX activation, suggesting that ABT-263-induced apoptotic cell death is mediated through BAX. Our in vivo studies also confirm senescence induction in tumor cells by cisplatin, and the promotion of apoptosis coupled with a significant delay of tumor growth after sequential treatment with ABT-263. Sequential treatment with cisplatin followed by ABT-263 extended the humane endpoint to ~130 days compared with cisplatin alone, where mice survived ~75 days. These results support the premise that senolytic agents could be used to eliminate residual senescent tumor cells after chemotherapy and thereby potentially delay disease recurrence in head and neck cancer patients.

SIGNIFICANCE STATEMENT

Disease recurrence is the most common cause of death in head and neck cancer patients. B-cell lymphoma-x large inhibitors such as ABT-263 (Navitoclax) have the capacity to be used in combination with cisplatin in head and neck cancer patients to eliminate senescent cells and possibly prevent disease relapse.

Introduction

Head and neck cancer is the sixth most common type of malignancy worldwide, with head and neck squamous cell carcinomas (HNSCCs) accounting for >90% of cases. HNSCC incidence largely correlates with tobacco and alcohol usage and is often diagnosed in advanced stages (Leemans et al., 2011). There is also a rapidly increasing incidence of a human papillomavirus-related (HPV+) subtype of HNSCC, which arises in a younger patient demographic that includes many never-smokers (Donà et al., 2020).

Head and neck cancer is generally treated with a combination of surgery, radiation, and chemotherapy, with cisplatin being a primary therapeutic modality (Cramer et al., 2019; Chow, 2020). Despite recent advances in cancer therapeutic approaches, 40% and 20% of patients with HPV-negative HNSCC experience locoregional and distant failure, respectively, after cisplatin-based chemoradiotherapy. While head and neck cancers are generally responsive to initial therapy, the disease almost invariably recurs, often becoming refractive to further therapy (Gibson et al., 2005; Argiris et al., 2008). An accumulating body of evidence has shown that cancer relapse often occurs after both conventional and advanced therapeutic approaches, where the therapy results in an accumulation of nonproliferative residual cancer cells (Goss and Chambers, 2010; Kareva, 2016). The cross talk between these tumor cells and their microenvironment can result in

This research was supported in part by the National Institutes of Health [Grant R03-CA235097] (to H.H.) and [Grant R01-CA239706] (to D.A.G. and H.H.) and the AADR Students Research Fellowship (to E.B.). Services and products generated by the VCU Massey Cancer Center Cancer Mouse Model Shared Resource were supported in part by funding from NIH National Cancer Institute (NCI) Cancer Center Support [Grant P30-CA016059].

A.J.S. and J.D.L. are employees and shareholders of AbbVie. A.C.F. is a paid consultant for AbbVie. Other authors have no actual or perceived conflict of interest with the contents of this article.

[1]F.A. and T.B. contributed equally to this work.

dx.doi.org/10.1124/molpharm.121.000354.

[S] This article has supplemental material available at mol.aspetjournals.org.

ABBREVIATIONS: BCL-2, B-cell lymphoma-2; BCL-X_L, B-cell lymphoma-x large; CHAPS, 3-[(3-Cholamidopropyl) dimethylammonio] 1-propanesulfonate; FACS, fluorescence-activated cell sorting; HNSCC, head and neck squamous cell carcinoma; 4NQO, 4-nitroquinoline 1-oxide; OSCC, oral squamous cell carcinoma; SA-β-gal, senescence-associated β galactosidase; SASP, senescence-associated secretory phenotype; VCU, Virginia Commonwealth University.

escape from the growth-arrested state via recovery of the cellular proliferative capacity, leading to disease recurrence (Sosa et al., 2014; Yeh and Ramaswamy, 2015).

The mechanisms whereby the residual cells maintain their long-term survival is poorly understood, but a significant number of recent studies have shown that transient senescence, the tumor cells' primary response to subtoxic doses of chemotherapy and/or radiation, can potentially contribute to cancer recurrence (Demaria et al., 2017; Duy et al., 2021). Senescence in cancer was first described as the limited proliferative capacity of tumor cells in response to activated oncogenes, oxidative stress, specific cytokines and chemokines, and DNA damage induced by chemicals such as chemotherapeutic agents (therapy-induced senescence) (Ewald et al., 2010). Senescence was originally considered to represent an irreversible form of growth arrest; however, studies in various cancer models including lung, prostate, and breast (Elmore et al., 2005; Roberson et al., 2005; Wang et al., 2013; Chitikova et al., 2014; Saleh et al., 2019) have shown that while therapy-induced senescence in cancer cells is durable, it does not actually represent a permanent form of growth arrest. Consequently, the senescence phenotype is not necessarily a favorable outcome of cancer therapy. In addition to cell cycle arrest, senescence is characterized by pronounced alterations in cells morphology, increased lysosomal biogenesis with β-galactosidase expression, facultative heterochromatin condensation and foci formation H3K9Me3 (SAHF), and secretion of various inflammatory cytokines and chemokines such as IL-6, IL-8, IL-1β, and MMP3, reflecting the senescence-associated secretory phenotype (SASP) (Sharpless and Sherr, 2015; Hernandez-Segura et al., 2018).

Senolytics are a relatively new class of drugs that have been shown to selectively induce cell death in senescent cells (Baker et al., 2011; Saleh et al., 2020b). One of the extensively characterized and effective senolytics is a B-cell lymphoma-2 (BCL-2) homology 3 mimetic, specifically the BCL-2 and BCL-X_L inhibitor known as ABT-263 (Navitoclax) (Saleh et al., 2020b). Navitoclax has been shown to have high affinity toward the hydrophobic pocket of antiapoptotic proteins such as BCL-2 and BCL-X_L (Chen et al., 2011). Upon binding, proapoptotic proteins such as BAX/BAK are released from these antiapoptotic proteins, resulting in the activation of proapoptotic BAX/BAK to initiate apoptosis by releasing cytochrome c from mitochondria to the cytosol followed by caspase activation (Mérino et al., 2012). Studies have shown that antiapoptotic BCL-2 family proteins are often overexpressed in cancer cells after chemotherapy or radiation, which is thought to be a central mechanism by which cancer cells survive beyond first-line therapies and, ultimately, lead to metastasis and cancer recurrence (Raffo et al., 1995). Navitoclax has demonstrated activities in investigational clinical trials both as a single agent and in combination with chemotherapy or radiation in different cancer types (Rudin et al., 2012; Puglisi et al., 2021).

The current studies demonstrated transient senescence induction by cisplatin in human and murine head and neck cancer cell lines and in head and neck cancer mouse models. Furthermore, escape from senescence was observed in experimental models of head and neck cancer whereas navitoclax was shown to have senolytic activity both in culture and in tumor-bearing animals. Mechanistic studies identified BCL-X_L as a primary target of navitoclax for the killing of senescent head and neck cancer cells. BCL-X_L was induced after cisplatin treatment, whereas navitoclax administration released BAX from the BCL-X_L/BAX complex to induce apoptosis specifically in senescent cells. Finally, sequential treatment with cisplatin followed by navitoclax significantly delayed tumor growth and prolonged survival in the mouse model of head and neck cancer.

Materials and Methods

Cell Lines and Drug Treatments. Investigations were carried out on two HPV-negative human HNSCC cell lines, HN30 (wild-type p53) and HN12 (truncated nonfunctional p53), which were provided by Dr. Andrew Yeudall (Augusta University). Cells were cultured in DMEM (Thermo Fisher, 10569010) supplemented with 10% (v/v) fetal bovine serum (Gemini, 26140), 100 U/ml penicillin G sodium and 100 μg/ml streptomycin sulfate (Thermo Fisher, 15140148) at 37°C and 5% CO_2. HN30 BAX and BAK knock-down cell lines were established by viral particles generated by HEK293T cells after co-transfection with appropriate shRNA plasmids, psPAX2 (addgene, 12260), and pMD2.G (Addgene, 12259) with EndoFectin-Lenti (GeneCopoeia, EF013). Next, viral supernatants were collected and used for HN30 cells transduction. Finally, transduced cells were selected by 2 μg/ml puromycin in several passages for a pure knocked-down population. Cisplatin (Sigma-Aldrich, 15663-27-1, ≥98% (HPLC) was dissolved in PBS, and ABT-263 (AbbVie Inc), ABT-199 (APExBio, A8194, 98.07% HPLC), and A-1155463 (APExBio, B6163, 98.78% HPLC) were dissolved in DMSO and administered in the dark at the desired concentrations. Drugs are stable after preparation and were kept at -20°C in the dark.

Cell Viability and Clonogenic Survival Assays. Cell viability was determined by monitoring the number of viable cells over time using trypan blue dye exclusion staining before, during, and after drug treatment. Cells were treated with 5 μM cisplatin for 24 hours and were collected by trypsinization at specific time points, then stained with 0.4% trypan blue (Sigma, T8154) and counted using hemocytometer under light microscopy. For clonogenic survival assays, cells were seeded at a low density at 5×10^3/10 cm dish or 1,000/6-well plates, then treated with 2 μM ABT-263, ABT-199, A-1155463 or vehicle for 24 hours. Colony formation was monitored over time, and at the experiment endpoint (at day 14, when the vehicle-treated condition formed distinct colonies with more than 50 cells) colonies were fixed with 100% methanol, air-dried, stained with 0.05% crystal violet, and counted using a colony counter (COLOCOUNT Discovery Technology Intl).

Senescence-Associated β Galactosidase Staining/Enrichment. Histochemical staining of senescence-associated β galactosidase (SA-β-gal) was performed as previously described (Dimri et al., 1995; Debacq-Chainiaux et al., 2009). Images were taken by a bright field inverted microscope (Olympus inverted microscope IX70, 20x objective, Q-Color3 Camera; Olympus, Tokyo, Japan). The C_{12}FDG flow cytometry was performed using the protocol described by Debacq-Chainiaux et al. (Debacq-Chainiaux et al., 2009). At the specific time points, cells were collected, washed with PBS, and analyzed by flow cytometry (using BD FACSCanto II and BD FACSDiva software at the Virginia Commonwealth University (VCU) Flow Cytometry Core Facility). Similarly, for immunofluorescent staining of C_{12}FDG, cells were exposed to 100 nM of bafilomycin A1 (Sigma Aldrich, B1793, >90% HPLC) for one hour, and after increasing the lysosomal PH, cells were exposed to 100 μM C_{12}FDG (Thermo Fisher, D2893) for 2 hours. After washing with PBS, nuclei were stained with Hoechst 33342 (Thermo Fisher, 33342) for 20 minutes in complete media. Images were taken using the Olympus inverted microscope. To enrich the senescent population, cells were seeded at high density for 1-2 × 10^6/150 mm dish and cultured overnight. The next day, cells were treated with cisplatin, and at the indicated time

points, they underwent C_{12}FDG staining as described above. Finally, cells were sorted by FACS. All the above experiments were performed at day 5 after treatment with 5 μM cisplatin for 24 hours.

Total Cell Lysates, Subcellular Fractionation, and Western Blotting. Total cell lysates were prepared using the CHAPS buffer [20 mM Tris (pH 7.4), 137 mM NaCl, 1 mM dithiothreitol (DTT), 1% CHAPS (3-[(3-Cholamidopropyl) dimethylammonio] 1-propanesulfonate)]. The mitochondria fraction was prepared with Qproteome Mitochondria Isolation Kit (Qiagen, 37612) according to the manufacture's protocol. Western blotting was performed as described (Sharma et al., 2014). Antibodies used in 1:1000 dilution included cleaved PARP (Cell Signaling, 5625), cleaved caspase-3 (Cell Signaling, 9664,), GAPDH (Cell Signaling, 5174), BCL-2 (Sigma, B3170), BCL-X_L (Cell Signaling, 2764), BAX (Cell Signaling, 2772), BAK (Cell Signaling, 12105), p53 (Santa Cruz, 23959), p21 (Cell Signaling, 2947), COX-IV (Cell Signaling, 4850).

Coimmunoprecipitation. BCL-X_L (Cell Signaling, 2764) or BAX (Santa Cruz, 23959) primary antibodies (1:100 dilution) were added to equal amounts of total lysates extracted from treated and nontreated cells. After an overnight incubation at 4°C, Protein A/G beads (Thermo Fisher, 53132) were added for 1 hour incubation at 4°C to precipitate the protein-antibody complexes. Samples were centrifuged, washed, and resuspended in 50/50 CHAPS buffer and 2X SDS-loading buffer. After boiling the samples for 5 minutes, they were subjected to SDS-PAGE followed by western blotting as described above.

Cell Cycle, Annexin-V/PI Staining, and γ-H2AX Analysis. Cell cycle analysis was performed based on propidium iodide staining (Saleh et al., 2019), and apoptosis quantification was done using AnnexinV-FITC apoptosis detection kit (556547, BD Biosciences, NJ, USA). Cells were seeded at the density of 4×10^4 cells per milliliter, treated with 5 μM cisplatin for 24 hours, and harvested at the indicated time points. After washing the samples with PBS, cells were resuspended in 100 μl of 1x Binding Buffer and incubated for 15 minutes in the dark at room temperature. Up to 500 μl of extra binding buffer was added to the final suspension and then the samples were analyzed by flow cytometry. Cell cycle analysis was performed at day 5 after treatment with cisplatin, and apoptosis was assessed at day 7. For γ-H2AX analysis, cells were seeded at a density of 4×10^4 cells per milliliter, treated with 5 μM cisplatin or vehicle for 24 hours. At day 5, 2 μM ABT-263 was added to the combination conditions for 48 hours and γ-H2AX induction was monitored by flow cytometry at day 7. Cells were harvested, fixed with 3.7% formaldehyde and permeabilized with cold methanol. After washing the pellets, cells were incubated with 1:250 dilution of γ-H2AX antibody conjugated to FITC [anti-H2AX (pS139), BD Biosciences, Cat. No. 560443] for 30 minutes.

Live-Cell Imaging. HN30 cells were plated (5×10^5 cells per milliliter) in 6-well plates and incubated overnight. After treatment with 5 μM cisplatin or vehicle for 24 hours, the plates were immediately placed on a CytoSMART digital microscopy system inside a humidified CO_2 incubator at 37°C. Live time-lapse images were taken every 15 minutes for 48 hours on day 5 (growth arrested and control cells, respectively) and day 10 (cells escaping from senescence and recovering their proliferative capacity).

Quantitative Reverse Transcriptase Polymerase Chain Reaction. Cells were plated (5×10^5 cells per milliliter) and treated with 5 μM cisplatin for 24 hours. At day 5 cells were harvested and total RNA was extracted using RNeasy kit (QIAGEN, 74004) following the manufacturer's instructions. cDNA was synthesized using iScript cDNA Synthesis Kit (BioRad, 4106228) based on the protocol that manufacture provided. cDNAs from different samples were amplified in technical triplicates using iTaq Universal SYBR Green Supermix (BioRad, 10000068167) in QuantStudio 3 Real-Time PCR System (Thermo Fisher). QuantiTect primers were purchased from Qiagen: CXCL8: QT0000322; IL-6: QT00083720; IL-1β: QT00021385; MMP3: QT00060025; GAPDH: QT00079247. Relative mRNA expression was determined using the ΔΔCt method.

In Vivo Experiments. All animal studies were conducted in accordance with VCU Institutional Animal Care and Use Committee (IACUC) guidelines. We first established the mouse oral squamous cell carcinoma (OSCC) cell line, 602, derived from the 4-nitroquinoline-1 oxide (4NQO)-developed tumor on the tongue. Female C57BL/6 mice (5 weeks of age; Envigo) were treated with 50 μg/ml 4NQO-containing water for 16 weeks. Then the drinking water was reverted to regular water until week 22. When a single lesion on the tongue became ~50 mm^3, a tumor was removed and digested, and cells were isolated to establish a cell line. To establish tumors, 1×10^6 of 602 OSCC cells were suspended in 50/50 PBS-Cultrex basement membrane matrix (Cultrex, 3632-005-02) and subcutaneously inoculated into the rear flanks of C57BL/6 female mice (day 0). When tumor size approached ~100 mm^3, mice were randomized in five groups (day 13, $N = 6$/group) and treated with cisplatin (5 mg/kg) by intraperitoneal injections at days 13, 16, 20 and 23, then with ABT-263 (80 mg/kg) by oral gavage daily at days 27-31 and daya 34-38. The second round of treatments was performed with cisplatin at days 41, 44 and 48, followed with ABT-263 at days 55-59 and days 62-66. Tumor volumes were taken by manual caliper measurements.

Immunohistochemistry. For cleaved caspase-3 (Cell Signaling, 9664) and γ-H2AX (Cell Signaling, 9718), tumors were fixed in 10% formalin phosphate buffer and performed on BOND RX Fully Automated Research Stainer. Slides were stained overnight at 4°C with cleaved caspase-3 (1:500) or γ-H2AX (1:400) primary antibodies then for 8 minutes at room temperature with the secondary antibody included in the BOND Polymer Refine Detection kit (Leica, DS9800). Slides were mounted with Dako CoverStainer (Agilent). Images were taken on Vectra Polaris Automated Quantitative Pathology Imaging System (Akoya Biosciences) at 20X at the VCU Cancer Mouse Models Core (CMMC). For X-Gal staining, tumors were frozen into OCT molds and cut into 10-micron sections by the VCU Tissue and Data Acquisition and Analysis Core (TDACC).

Blood Analysis and Platelet/Neutrophil Counts. Mice treated with vehicle, cisplatin, ABT-263, or a combination of cisplatin and ABT-263 were subjected to complete blood count analysis at the indicated time points (Fig. 6E). Blood samples (~0.2 ml) were collected by facial vein using EDTA coated syringes and immediately analyzed by hematology analyzer Hemavet 950FS (Drew Scientific, Miami Lakes, FL, USA) at the VCU Cancer Mouse Models Core.

Statistical Analysis. Unless otherwise indicated, all quantitative data are shown as mean ± S.D. from at least three independent experiments (biologic replicates), all of which were conducted in triplicates or duplicates (technical replicates). GraphPad Prism 6.0 software was used for statistical analysis. All data were analyzed using either a one- or two-way ANOVA, as appropriate, with Tukey or Sidak post hoc, except for cell cycles, C_{12}FDG data, and platelet counts, which were analyzed with unpaired, student's t tests.

Results

Cisplatin Induces Growth Arrest and Senescence in Head and Neck Cancer Cells. Pharmacokinetic studies have indicated that the highest plasma concentration of cisplatin achieved in patients is 12 μM at 5 minutes after injection, while the plasma concentration decreases to 5.9 μM after 2 hours. Up to 90% of total cisplatin is excreted (depending on the patient's renal function) in 24 hours. Consequently, initial experiments to investigate the cellular response to cisplatin in head and neck cancer cells involved exposure to clinically relevant concentrations of cisplatin (2, 5, and 10 μM) for 24 hours (Farris et al., 1988; Urien and Lokiec, 2004; Ang et al., 2014). As expected, cisplatin induced a temporary growth arrest after 24 hours of treatment in both HN30 (p53 wild-type) and HN12 (p53-null) head and neck cancer cell lines. As we have reported in other tumor

cell models (Saleh et al., 2019; Saleh et al., 2020b), the cells ultimately escaped and recovered their proliferative capacity (Fig. 1A). Cell cycle analyses confirmed that both cell lines arrested primarily at the G0/G1 phase (Fig. 1B).

The antitumor activity of cisplatin is generally ascribed to the induction of DNA single- and double-strand breaks caused by the cross-linking of DNA (Jeon et al., 2008; Basu and Krishnamurthy, 2010; Rezaee et al., 2013). Consistent with the fact that senescence has been suggested to be the primary response of tumor cells to chemotherapeutic agents and cellular stress conditions (Triana-Martínez et al., 2020), we confirmed that cisplatin promotes senescence in our experimental models. This determination was based on several characteristics, such as morphologic changes, qualitative and quantitative measurement of SA-β-gal activity using X-gal staining (Fig. 1C, upper portion) and fluorescence-based labeling with C_{12}FDG (Fig. 1C, right panels, and Supplemental Fig. 1), and upregulation of the tumor suppressor p53 and the cyclin-dependent kinase inhibitor p21 (Fig. 1D). Additional senescence markers, specifically heterochromatic foci (H3K9Me3) formation (Fig. 1C, lower panels) and increased expression of Senescence-Associated Secretory Phenotype (SASP) components such as *IL-6, IL-8, and IL-1β* (Fig. 1E), further confirmed that cisplatin treatment can promote senescence in HNSCC cells regardless of the *p53* status.

Proliferative Recovery in Cisplatin-Treated HNSCC Cells Is Associated with a Decline in Senescence Markers. Despite the long-held paradigm that therapy-induced senescence (TIS) is an irreversible and permanent form of growth arrest, which would be consistent with a favorable therapeutic outcome of senescence induction (Shay and Roninson, 2004), our previous studies, along with rigorous

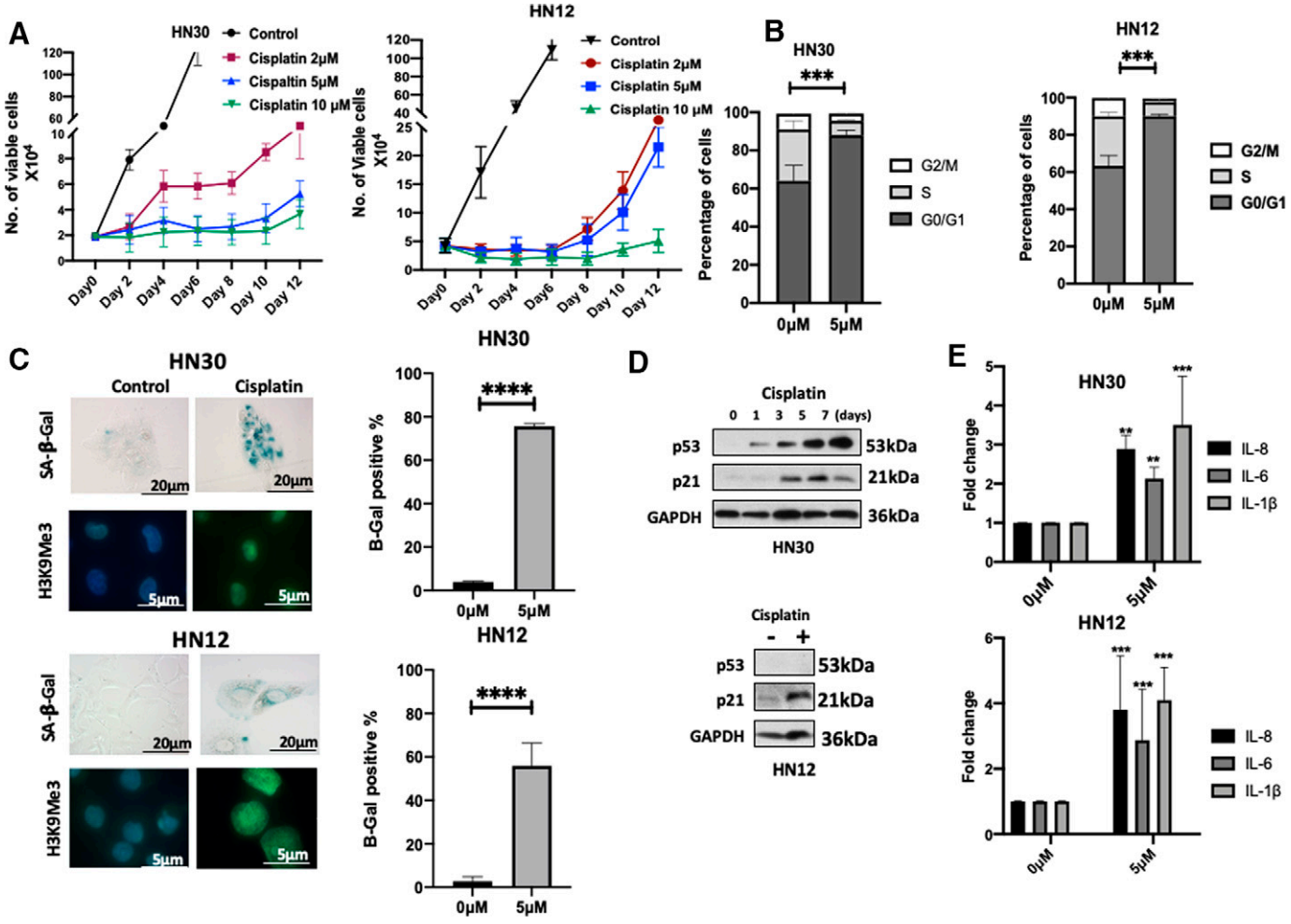

Fig. 1. Cisplatin induces senescence-mediated growth arrest in HNSCC cells. (A) Cell viability was monitored over a period of 12 days by trypan blue exclusion in HN30 and HN12 cells after 24 hours of exposure to 2, 5, and 10 μM cisplatin. (B) Cell cycle analysis of HN30 and HN12 cells at day 5 after treatment with 5 μM cisplatin for 24 hours. Cell cycle distribution is shown in the bar graphs. * $P \leq 0.05$, ** $P \leq 0.01$, *** $P \leq 0.001$, **** $P \leq 0.0001$ indicate statistical significance of each condition compared with control as determined using Student's t-test. (C) Cells were analyzed for increased expression of SA-β-gal using X-gal (20x objective, scale bar: 20 μm, bright field images) or C_{12}FDG (bar graphs) and increased SAHF formation by H3K9ME3 immunofluorescence (100x objective, scale bar: 5 μm, fluorescent images). Blue fluorescence indicates nuclear staining with 4′,6-diamidino-2-phenylindole, and green fluorescence reflects H3K9Me3 immunostaining. Staining was performed 5 days after treatment with 5 μM cisplatin for 24 hours. (D) Western blotting for p53 and p21 in HN30 and HN12 cells at the indicated time points after cisplatin treatment. (E) qRT-PCR for the SASP mRNAs IL-6, IL-8, and IL-1β. RNA was extracted at day 5 following cisplatin exposure. All images are representative fields or blots from at least three independent experiments, and all quantitative graphs are mean ± S.D. from at least three independent experiments. * $P \leq 0.05$, ** $P \leq 0.01$, *** $P \leq 0.001$, and **** $P \leq 0.0001$ indicate statistical significance of each condition compared with control as determined using two-way ANOVA with Sidak's post hoc test. All images are representative fields or blots from three independent experiments ($n = 3$).

experiments by other investigators, have firmly established that at least a subpopulation of cells can and will evade the senescent arrest and re-emerge with self-renewal capacity (Elmore et al., 2005; Roberson et al., 2005; Puig et al., 2008; Wang et al., 2013; Chitikova et al., 2014; Saleh et al., 2020b). To interrogate whether this is also the case for head and neck cancer cells induced into senescence by cisplatin, we used multiple approaches to investigate the capacity for proliferative recovery from senescence in our experimental models. Live-cell imaging microscopy was used to monitor proliferative recovery from cisplatin-induced senescent HN30 cells (Supplemental Videos 1A, B, and C). A comparison of the morphologic characteristics of cells at different time points established that the emerging population at day 11 in Supplemental Video 1C was indeed derived from the senescent population. Further confirmation of the involvement of senescence in recovery was based on the observation that proliferative recovery in our models is associated with diminution of the senescence markers (Fig. 2). Specifically, SA-β-gal activity showed a significant reduction after the cells recovered their proliferative capacity (Fig. 2A). Similarly, the decline in additional senescence markers such as components of the senescence-associated secretory phenotype (SASP) (Fig. 2B) further indicates that the cisplatin-induced senescent-like state is not sustained.

It is possible that the recovered population originated from a subclone that was resistant to the primary effects of cisplatin de novo rather than escape from chemotherapy-induced senescence (Beauséjour et al., 2003; Dirac and Bernards, 2003). To confirm that cells can and do recover from chemotherapy-induced senescence, cisplatin-induced senescent cells were labeled with the fluorescent substrate of SA-β-gal, C_{12}FDG, and enriched for the highest ~30% of the C_{12}FDG-positive (SA-β-gal-positive) and morphologically enlarged population using fluorescence-activated cell sorting (FACS). This protocol ensures a highly specific and selective purification of senescent population from a heterogeneous mixture of tumor cells after treatment. The highly C_{12}FDG-positive population was then re-plated and monitored for senescence markers such as proliferative arrest, and SA-β-gal activity. As shown in Fig. 2, C and D, the sorted

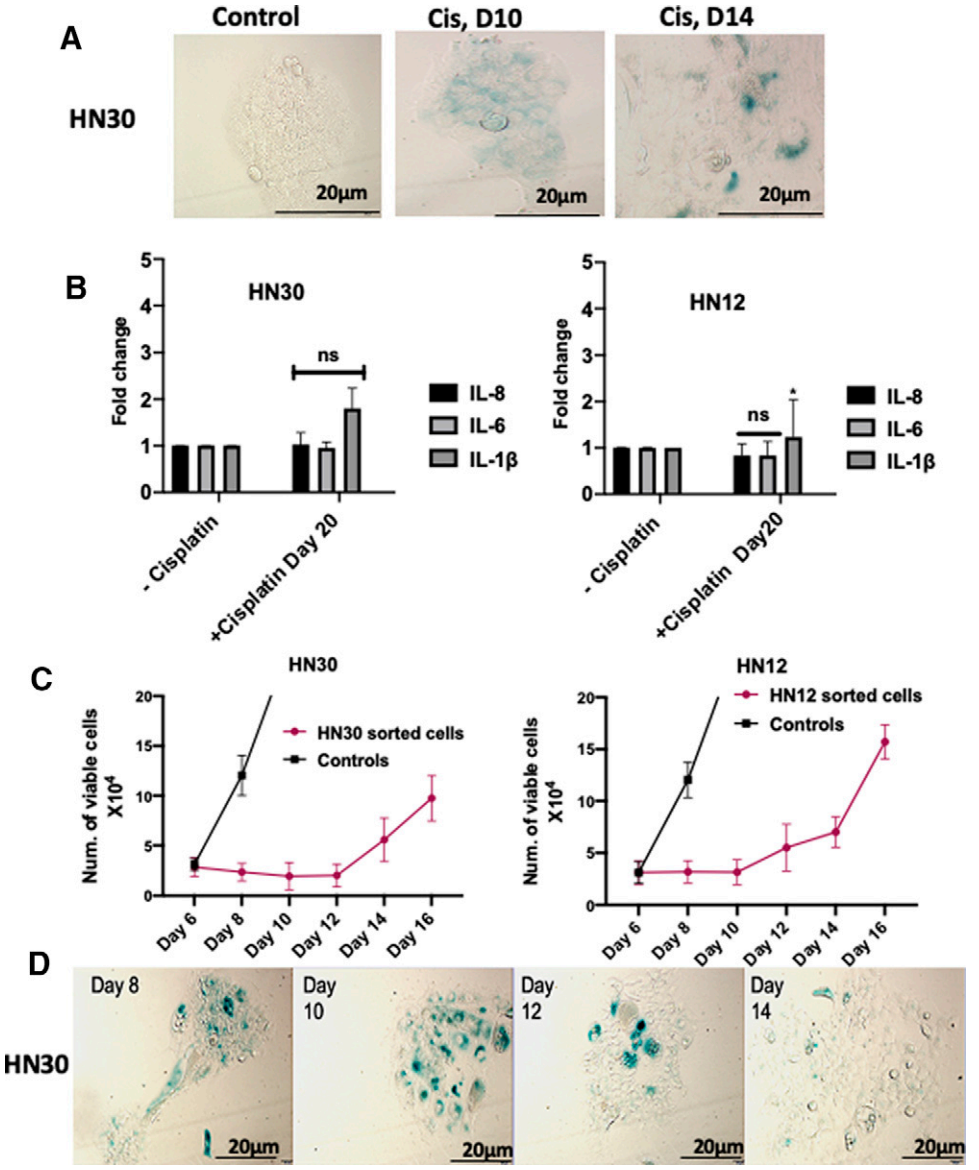

Fig. 2. Proliferative recovery from cisplatin treatment in HN30 and HN12 cells is associated with the reduction of senescence-associated features. (A) Histochemical SA-β-gal staining (20x objective, scale bar: 20 μm, bright field images). Cells were treated with 5 μM cisplatin for 24 hours and stained for SA-β-gal activity at days 10 and 14. Note that the enzyme activity declines with cellular proliferative recovery. (B) qRT-PCR for the SASP mRNAs IL-6, IL-8, and IL-1β. *$P \leq 0.05$, **$P \leq 0.01$, and ***$P \leq 0.001$ indicate statistical significance of each condition compared with control as determined using two-way ANOVA with Sidak's post hoc test. (C) Growth curve and (D) SA-β-gal staining for high-C_{12}FDG-positive HN30 and HN12 cells (enriched on day 5 after cisplatin treatment).

population recovered proliferative capacity after 16 days accompanied by the suppression of SA-β-gal activity.

ABT-263 Selectively Eliminates Senescent Tumor Cells In Vitro. The proliferative recovery in tumor cells re-emerging from a therapy-induced senescent population has been shown to contribute not only to recurrence of a more aggressive form of the disease, but also to acquired resistance to chemotherapy or radiation (Rebbaa, 2005; Yang et al., 2017). Consequently, in an effort to eliminate the cisplatin-induced senescent population, cisplatin-treated HN30 and HN12 cells were exposed to a single dose of ABT-263, an agent that has demonstrated senolytic properties (Sharma et al., 2014; Lafontaine et al., 2021) for 24 hours. A significant decrease in the number of viable cells (Fig. 3A) strongly suggests that ABT-263 selectively eliminates cisplatin-treated senescent cells, while showing minimal effects on untreated cells. Clonogenic survival assays using increasing concentrations of ABT-263 on untreated tumor cells confirmed that ABT-263 alone, even at higher concentrations, was ineffective in perturbing colony formation for nonsenescent tumor cells (Supplemental Fig. 2A). This result was recapitulated with selective inhibitors of BCL-2 (ABT-199) and BCL-X_L (A-1155463) (Supplemental Figs. 2B and 2C). In addition, ABT-263 treatment resulted in a significant decrease in the SA-β-gal positive (senescent) population (Supplemental Fig. 2D), further confirming the selective activity of ABT-263 for the senescent population. As we have reported previously in models of non-small cell lung cancer and breast cancer (Alotaibi et al., 2016; Saleh et al., 2019), ABT-263 effectiveness diminishes over time as the treated cells escape senescence and recover their proliferative capacity (Supplemental Fig. 2E, lower panel) in marked contrast to the effectiveness of ABT-263 after a second dose of cisplatin (Supplemental Fig. 2E, upper panel). This observation reaffirms the selectivity of ABT-263 for a senescent cell population.

Consistent with previously published studies on ABT-263 as an apoptosis-inducing agent (Tse et al., 2008), there was a significant increase in Annexin-V/PI staining and the apoptosis marker, cleaved caspase-3, in the combinatorial treatment group (cisplatin followed by ABT-263) compared with cisplatin or ABT-263 alone (Figs. 3B and 3C). Taken together, these observations strongly confirm that ABT-263 acts as a selective senolytic in vitro by significantly decreasing the number of cisplatin-induced senescent cells.

The BCL-X_L/BAX Axis Is the Primary Target for Cell Death Induced by ABT-263 in Cisplatin-Induced Senescent HNSCC Cells. ABT-263 is known to specifically inhibit the function of the antiapoptotic BCL-2 and BCL-X_L proteins to induce apoptotic cell death (Tse et al., 2008). To delineate the specificity of the inhibitory activity in head and neck cancer, we treated cisplatin-induced senescent HN30 cells with a BCL-2-specific inhibitor, ABT-199, and a BCL-X_L-specific inhibitor, A-1155463. These agents do not have an effect on nonsenescent HN30 cells (Supplemental Figs. 3A, 3B, 2A, 2B, and 2C). However, A-1155463, but not ABT-199, eliminated senescent cells, suggesting that BCL-X_L is the primary target in senescent HNSCC cells (Fig. 4A; Supplemental Fig. 3A). We further confirmed that ABT-263 and A-1155463-mediated cell death was occurring primarily via apoptosis using

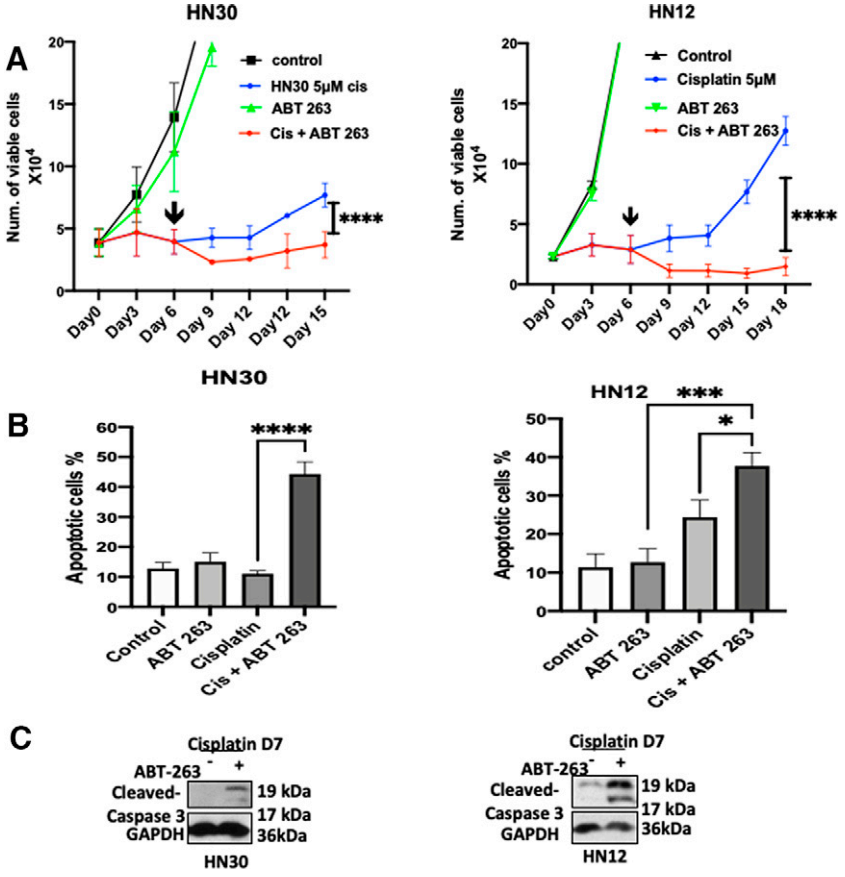

Fig. 3. ABT-263 induces apoptotic cell death in cisplatin-induced senescent cells. (A) Growth curves for cells treated with cisplatin followed by either vehicle or 2 μM ABT-263 for 24 hours. Arrows indicate the time of ABT-263 treatment. (B) Annexin-V/PI quantification of apoptosis induced by 2 μM ABT-263 with overnight exposure 24 hours after drug removal (day 7) in HN30 and HN12 cells after treatment with cisplatin. (C) Western blots for cleaved caspase-3 in HN30 and HN12 cells. Cells were treated with 5 μM cisplatin followed by ABT-263 for 24 hours and harvested at day 7. All images are representative fields or blots from at least three independent experiments, and all quantitative graphs are mean ± S.D. from at least three independent experiments. * $P \leq 0.05$, ** $P \leq 0.01$, *** $P \leq 0.001$, and **** $P \leq 0.0001$ indicate statistical significance of each condition compared with control as determined using two-way ANOVA with Sidak's post hoc test.

Annexin-V staining (Fig. 4C). Similar specificity to BCL-X_L was also observed in p53-null HN12 cells (Figs. 4B, 4D, and Supplemental Fig. 3B). These results strongly suggest that BCL-X_L is the primary target of ABT-263-induced senolytic cell death.

To further support that the senolytic activity of ABT-263 in head and neck cancer cells was driven by inhibition of BCL-X_L, we next determined the expression of major BCL-2 family proteins in cisplatin-induced senescence HN30 cells. The level of the antiapoptotic protein, BCL-X_L, gradually increased following cisplatin treatment (Fig. 5A). Consistently, these increases were also observed in the HN12 cells (Fig. 5B). Changes of other BCL-2 family proteins were inconsistent (Figs. 5A and 5B).

ABT-263 inhibits the interaction of BCL-X_L with BAX/BAK, thereby inducing apoptosis (Saleh et al., 2020b). To elucidate the involvement of these executioner pro-apoptotic proteins following ABT-263 treatment, we established stable HN30 cells with shRNA for BAX (shBAX), BAK (shBAK), or scrambled-control (shC) (Fig. 5C). Although these cell lines undergo similar induction of senescence following exposure to cisplatin (Fig. 5D, bottom), cisplatin-treated shBAX-expressing cells, but not shBAK expressing cells, failed to undergo cell death following exposure to ABT-263 (Fig. 5D, top), indicating that BAX is essential to ABT-263-induced senolysis.

The above results prompted us to investigate the subcellular localization of BAX and BCL-X_L, their interaction, and BAX conformational change/activation. The mitochondria-enriched lysates revealed the accumulation of BAX in cisplatin-induced senescent and further in ABT-263-treated HN30 cells (Fig. 5E). In contrast, the amounts of BCL-X_L and BAK at the mitochondria were only modestly perturbed (Fig. 5E). We then investigated the BCL-X_L/BAX interaction by co-immunoprecipitation experiments. When BCL-X_L was immunoprecipitated, BAX was present in both the control and cisplatin treatment groups. However, when ABT-263 was introduced, the BCL-X_L/BAX interaction was significantly decreased (Fig. 5F), suggesting that ABT-263 inhibits the BCL-X_L/BAX interaction and releases BAX from the complex. This result indicated that BAX became activated to allow apoptosis to occur.

ABT-263 Selectively Eliminates Cisplatin-Induced Mouse Oral Squamous Cell Carcinoma Cells In Vitro and In Vivo. To test the senolytic activity of ABT-263 in vivo, we first established the mouse oral squamous cell carcinoma (OSCC) cell line (602) derived from the 4-nitroquinoline-1 oxide (4NQO)-developed tumor on the tongue (see *Materials and Methods*). A crystal violet and senescence-associated-β-galactosidase (SA-β-gal) stain revealed that cisplatin induced 602 cells into senescence and sensitized the cells to ABT-263 (Fig. 6A). We then evaluated senolytic activity of ABT-263 in a syngeneic mouse model. Cisplatin treatment resulted in brief tumor stasis compared with the control and ABT-263 monotherapy (Fig. 6B). Sequential cisplatin and

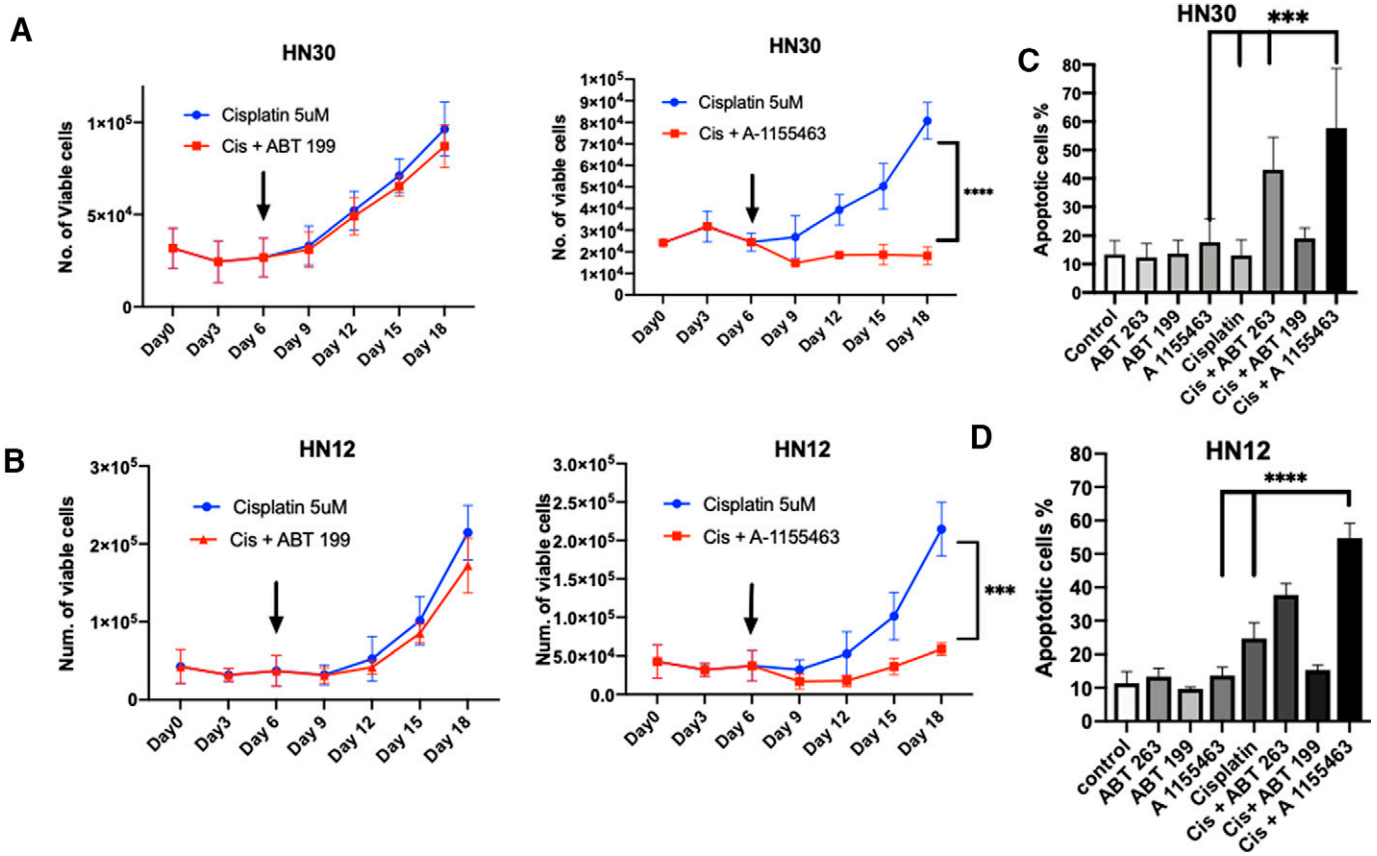

Fig. 4. BCL-X_L is the primary target for ABT-263-induced senolysis. Growth curves for (A) HN30 and (B) HN12 cells treated with 5 μM cisplatin followed by either vehicle, 2 μM A-1155463 (left) or ABT-199 (right) for 24 hours. Arrows indicate timepoints of A-1155463 or ABT-199 treatment. (C) and (D) Apoptotic cell death was determined in HN30 and HN12 cells, respectively, by Annexin-V/PI staining followed by FACS analysis. *** $P \leq 0.001$ and **** $P \leq 0.0001$ indicate statistical significance of each condition compared with indicated condition as determined using two-way ANOVA with Sidak's post hoc test.

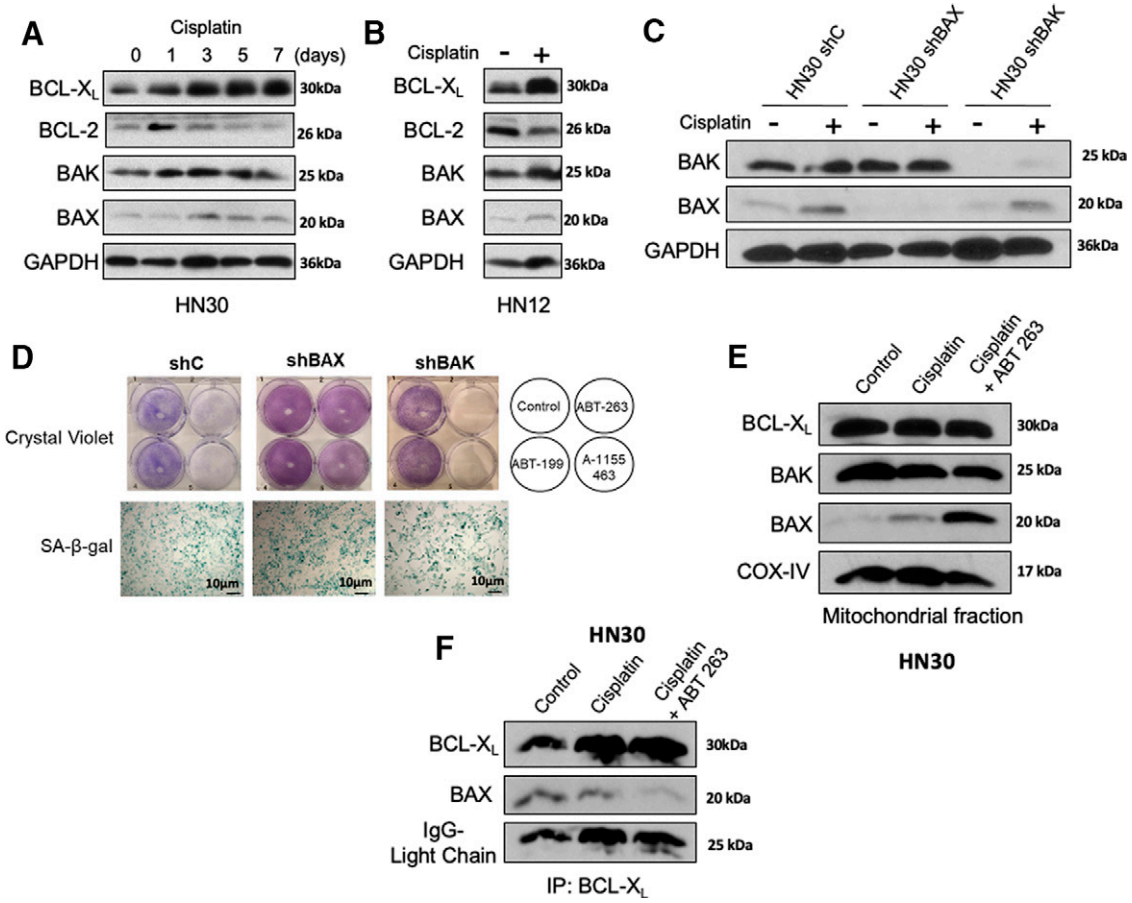

Fig. 5. ABT-263 induces senolytic activity through modulation of the BAX/BCL-X_L interaction. (A) HN30 cells were treated with cisplatin and harvested at the indicated times. (B) HN12 cells were treated with 5 μM cisplatin and harvested at day 7. Total cell lysates were subjected to western blotting with the indicated antibodies. (C) HN30 shBAX, shBAK, and shC (scrambled control) cells were treated with cisplatin (5 μM) for 5 days. Total cell lysates were subjected to western blotting with the indicated antibodies. (D) Senescent cells in (C) were treated with ABT-263, ABT-199, and A-1155463 (1 μM each) for 24 hours and stained with trypan blue and X-gal activity. (10x objective, scale bar: 10 μm, bright field images). (E) BAX is recruited to the mitochondria membrane upon ABT-263 treatment. HN30 cells were treated with cisplatin (5 μM) for 5 days followed by ABT-263 (1 μM) for 16 hours. The earlier time point allowed us to detect navitoclax effects on apoptosis regulatory proteins before apoptosis completion, which might have resulted in the degradation of select proteins. Mitochondria-enriched (heavy membrane) fractions were subjected to western blotting with the indicated antibodies. (F) ABT-263 disrupts the interactions of BCL-X_L and BAX. HN30 cells were treated as in (E), and total cell lysates were immunoprecipitated with anti-BCL-X_L antibodies followed by western blotting with the indicated antibodies. All images are representative fields or blots from three independent experiments ($n = 3$), and all quantitative graphs are mean ± S.D. from three independent experiments ($n = 3$).

ABT-263 treatment resulted in a distinct therapeutic benefit characterized by delayed tumor recurrence and longer survival (Fig. 6, B and C). Furthermore, two rounds of cisplatin followed by ABT-263 treatment (combination B) outperformed all groups, including the single round of cisplatin followed by ABT-263 (combination A), in terms of delayed tumor recurrence and improved animal survival. Animal experiment diagram is presented in Supplemental Fig. 4.

We further extracted and analyzed the 602 tumors to evaluate markers of senescence and the senolytic activity of ABT-263. Cisplatin-induced senescence in tumors in vivo was clearly detected as X-gal staining with increased SA-β-gal activity, which was then decreased upon ABT-263 treatment (Fig. 6D, left panels). Cisplatin also induces DNA single- or double-strand breaks (DSBs). The phosphorylated form of histone H2AX (γ-H2AX) marks sites of DNA DSB repair. Compared with the control, γ-H2AX was strongly stained in tumors exposed to cisplatin (Fig. 6D, middle panels). However, ABT-263 did not appear to alter the levels of γ-H2AX either alone or in combination with cisplatin, both in the tumor bearing animal experiments (Fig. 6D), and in the cell culture studies (Supplemental Fig. 5). Extensive cleavage of caspase-3 (c-casp3), indicative of apoptosis, was evident in tumors treated with cisplatin followed by ABT-263 (Fig. 6D, right panels). These results suggest that the benefit of sequential treatment is a result of apoptosis caused by ABT-263 in cisplatin-induced senescent tumors.

Based on the previous preclinical data in animal models (Shoemaker et al., 2006), ABT-263 treatment results in rapid and concentration dependent thrombocytopenia that resolves after drug cessation (Oltersdorf et al., 2005; Roberts et al., 2009). Here, we evaluated the safety of ABT-263 is our animal model by analyzing complete blood counts, particularly by focusing on the dynamic of circulating platelets and neutrophils (Fig. 7 and Supplemental Fig. 6). The number of circulating platelets and neutrophils in the different groups of

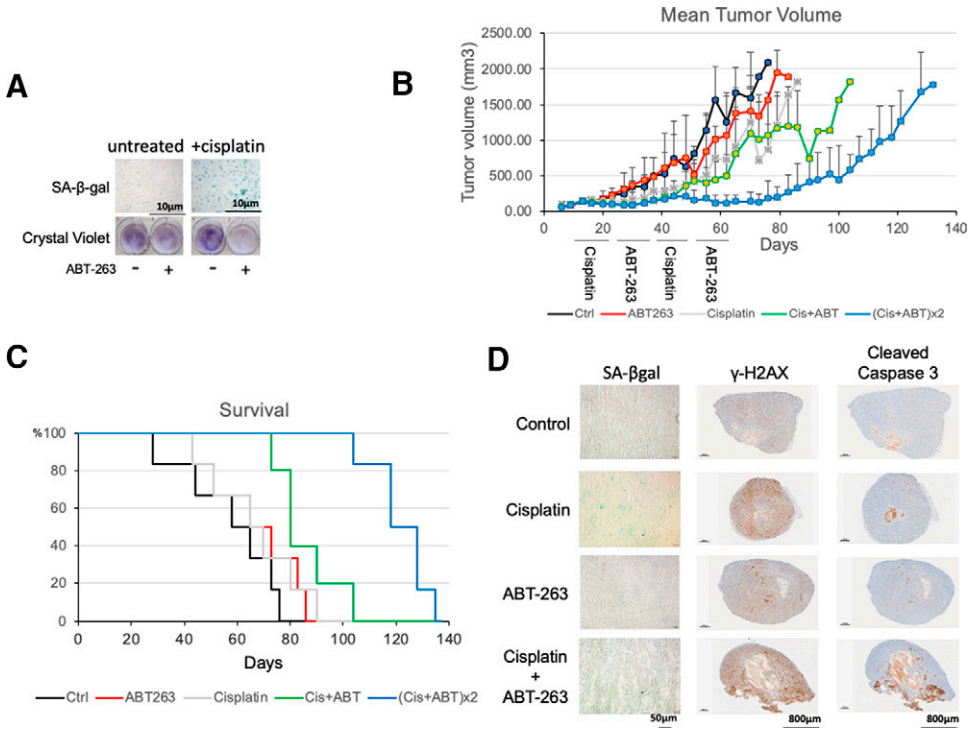

Fig. 6. Sequential administration of ABT-263 following cisplatin delays tumor recurrence in a syngeneic mouse model of OSCC. (A) ABT-263 eliminates cisplatin-induced senescent mouse OSCC cells in vitro. Mouse OSCC 602 cells were treated with cisplatin (2.5 μM, the dose efficiently induces senescence in this cell line) for 5 days followed by exposure to ABT-263 (1 μM) for 24 hours. Cells were stained with trypan blue to investigate ABT-263 effectiveness. X-gal staining in SA-β-gal-positive cells indicates senescence after cisplatin treatment (10x objective, scale bar: 10 μm, bright field images). (B) 602 cells were subcutaneously inoculated in C57BL/6 mice at the flank (day 0). When tumors achieved a size of ~100 mm^3, mice were randomized into five groups (day 13, N = 6/group). Mice were treated with cisplatin (5 mg/kg) at days 13, 16, 20, and 23, followed by ABT-263 (80 mg/kg) daily at days 27-31 and days 34-38. The second round of treatments was performed with cisplatin at days 41, 44, and 48, followed with ABT-263 at days 55-59 and days 62-66. Tumor volume (B) was determined by caliper measurements and survival (C) was monitored by Kaplan-Meier curves. (D) Tumors were excised after treatment with vehicle (control), cisplatin, ABT-263, or cisplatin followed by ABT-263. SA-β-gal activity was monitored by staining with X-gal, and DNA double-strand breaks repair and apoptosis were monitored by immunohistochemical staining with antibodies against γ-H2AX and cleaved-caspase-3, respectively (Original magnification = 20X). Graphs are represented as mean ± SEM. All tumor images are representative fields from four tumor slices (n = 3) taken from three mice per group (n = 3).

mice show that ABT-263 treatment alone or in combination with cisplatin does not result in thrombocytopenia or neutropenia in our experimental model system.

Discussion

Locoregional and distant recurrence are the most common causes of death in HNSCC patients, and it has been suggested that the morbidity and mortality is mediated by the progression from residual tumor cells that survive from the assault of chemotherapy or radiotherapy (Lambrecht et al., 2009). Similar contributions to recurrence from residual tumor cells are also observed in breast, prostate, and lung cancers. More specifically, whereas the initial therapies result in both tumor regression and stasis, a residual cell population can proliferate at secondary local or distant sites with equal or more aggressiveness (Morgan et al., 2009; Walens et al., 2019; Wu et al., 2020). This residual and dormant cell population could potentially be linked to senescent and quiescent tumor cells, as well as cancer stem cells (Kim et al., 2012; Wang et al., 2017; Phi et al., 2018).

Despite the fact that therapy-induced senescence has been investigated for decades, the contribution of senescent tumor cells to disease recurrence is still obscure (Pérez-Mancera et al., 2014). The senescence phenotype was initially considered as a favorable outcome of cancer therapy, as it likely represents a primary response to chemotherapy or radiation and cells in this state manifest characteristics such as prolonged growth arrest, which may lead to tumor regression (Nardella et al., 2011). However, as senescent cells are metabolically active and resistant to apoptosis (Seluanov et al., 2001; Wiley et al., 2017), it is anticipated that the considerable heterogeneity of senescent tumor populations would allow for proliferative recovery of some tumor subpopulations from the state of growth arrest (Hernandez-Segura et al., 2017; Wiley et al., 2017). Additionally, the ability of senescent cells to secrete proinflammatory cytokines and chemokines (SASPs) contributes to chronic inflammation and adverse paracrine effects (Krizhanovsky et al., 2008; Coppé et al., 2010). Finally, the tumorigenic potential and more aggressive behavior of post-senescent cells, including frequent epithelium-to-mesenchymal transition (EMT) and genomic instability, argues for the central involvement of senescent cells in disease recurrence (Sieben et al., 2018). To combat these potentially deleterious long-term effects of therapy-induced senescence, a new class of compounds, termed "senolytics," which selectively induce cell death in senescent cells, has been developed (Sieben et al., 2018).

In the current work, we investigated the utility of a two-hit sequential treatment approach, first with chemotherapy followed by senolysis, in head and neck cancer. We chose p53 wild-type HN30 cell line derived from pharynx and p53-null

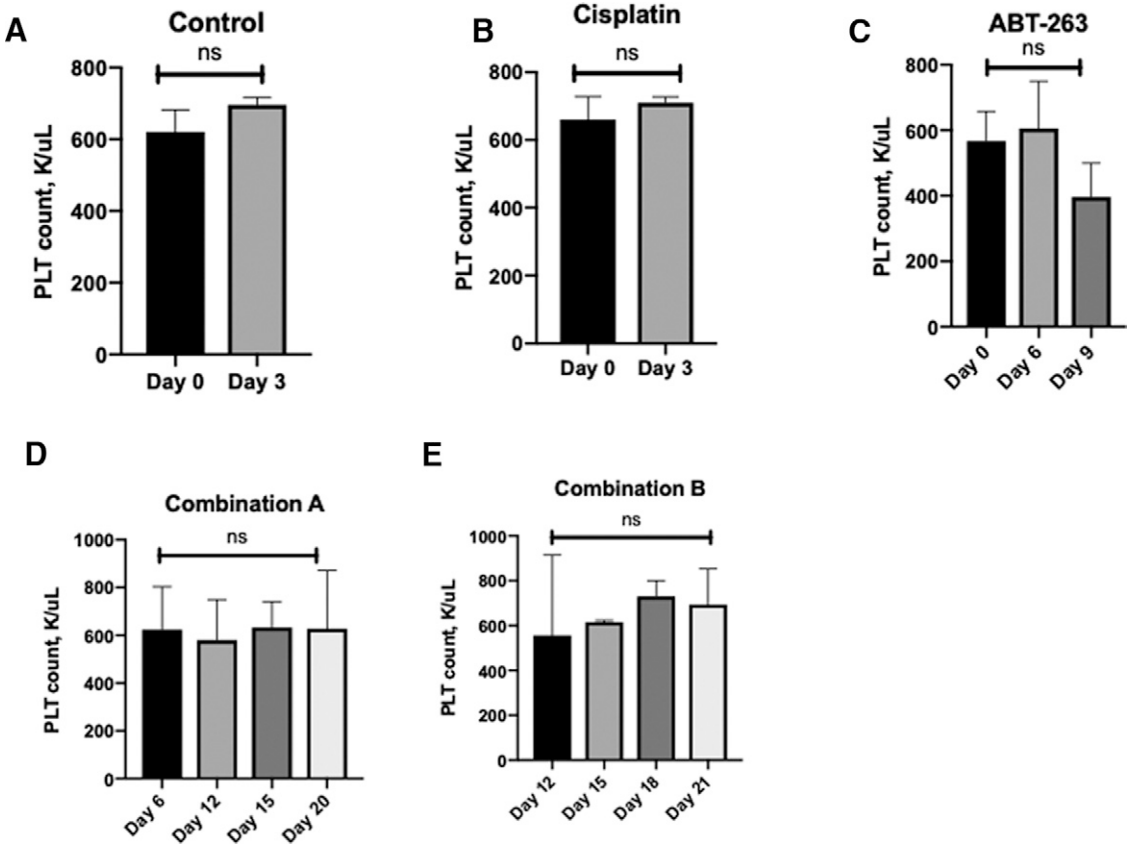

Fig. 7. Platelet cell count (K/μl) in mice treated with (A) vehicle, (B) cisplatin alone, (C) ABT-263 alone or (D) and (E) in combination with cisplatin over a period of 21 days. Control versus ABT, cisplatin, combination A or B: $P > 0.05$ as determined using two-way ANOVA with Sidak's post hoc test. All quantitative graphs are mean ± S.D. from at least three independent experiments.

HN12 cell line derived from lymph node metastasis (Singchat et al., 2016), in consideration of the fact that p53 is most commonly mutated in head and neck cancer patients (Leemans et al., 2011). Both cell lines showed a significant degree of senescence upon treatment with cisplatin by assessing multiple assays and markers (Fig. 1). The delayed senescence in HN12 cell line likely reflects the p53-independent pathway (Mirzayans et al., 2012). For example, it has been shown that p16 plays a critical role in senescence induction in p53-null models (Mirzayans et al., 2012). We also confirmed senescence and tumor stasis induced by cisplatin treatment in a syngeneic mouse model (Fig. 6, B and D). Furthermore, the proliferative recovery from senescence was confirmed using fluorescence-activated cell sorting (FACS) and live-cell imaging (Fig. 2 and Supplemental Videos) as well as in a mouse model (Fig. 6B). These results further support the recent paradigm shift that therapy-induced senescence is transient, but not permanent, growth arrest, which may contribute to tumor recurrence from dormancy (Saleh et al., 2020a).

To overcome the survival mechanism senescent cells maintain, our data indicates that a BCL-2/BCL-X_L inhibitor, ABT-263 (navitoclax), efficiently induces apoptosis following cisplatin treatment in in vitro and in vivo head and neck cancer models (Figs. 3 and 6D). These studies are consistent with previous reports showing effectiveness of ABT-263 in breast, lung, and prostate tumors (Zhu et al., 2015, 2016; Yosef et al., 2016; Grezella et al., 2018; Yabluchanskiy et al., 2020; Carpenter et al., 2021). We extensively investigated the selectivity of ABT-263, determining that this compound induces apoptosis only in the cisplatin-induced senescence population, but not in the proliferating population (Saleh et al., 2020b) (Fig. 3 and Supplemental Figs. 2A, 2B, and 2C). Additionally, our growth curve data with multiple exposures to cisplatin after proliferative recovery confirms that ABT-263 shows selectivity for the cells that are exposed to a second dose of cisplatin after recovery, but not the population recovered from the first cisplatin exposure (Supplemental Fig. 2E).

In mechanistic studies, we showed that (i) BCL-X_L is the primary target for apoptosis induced by ABT-263 in senescent cells (Fig. 4), and (ii) the inhibition of BCL-X_L/BAX interaction by ABT-263 followed by BAX activation is critical for this apoptosis induction (Fig. 5). We and others have shown that BCL-X_L expression increases gradually after senescence induction (Hayward et al., 2003; Saleh et al., 2020b; Mas-Bargues et al., 2021) and the sensitization induced by ABT-263 is BCL-X_L-dependent in breast and lung tumors (Saleh et al., 2020b). Our results indicate that BAX, but not BAK, is a critical proapoptotic protein for ABT-263-induced apoptosis in senescent cells in which the level of BCL-X_L is induced and BAX is accumulated at the mitochondria. It has been shown that an increase of BCL-X_L levels by overexpression leads to an increase of BAX at the mitochondria and sensitizes cells treated with ABT-737, a prototype BCL-2/BCL-X_L inhibitor of ABT-263, to apoptosis (Renault et al., 2015). We speculate that the physiologic levels of BCL-X_L increased by senescence induction also led to BAX accumulation at the mitochondria, which shifts the dependency of ABT-263-induced apoptosis toward BAX. Consistently,

studies have shown that BCL-X_L is qualitatively and quantitively ten times more active than BCL-2 and is more effective in apoptosis inhibition (Wang et al., 2004; Fiebig et al., 2006). Moreover, the majority of head and neck cancer patients' tumor biopsies have shown a significant upregulation in BCL-X_L, but not BCL-2 protein levels. BCL-X_L levels were shown to be directly associated with worse therapy outcomes, whereas BCL-2 positive tumors, even after locoregional metastasis, demonstrated better therapy outcomes (Pena et al., 1999). Carter et al. also showed that BCL-X_L is significantly overexpressed in head and neck cancer patients' tumor samples, while BCL-2 levels did not show any increase (Carter et al., 2019). These data suggest that BCL-X_L would play a major role, particularly in head and neck cancer, for drug sensitivity and treatment outcome. However, additional work is needed to define the precise role(s) of BCL-X_L and BCL-2, since our findings in this report, along with other publications in this area, clearly show that BCL-2 and BCL-X_L are functionally distinct.

Our data with a syngeneic mouse model (Fig. 6) clearly indicate that two rounds of sequential cisplatin followed by ABT-263 treatment has a distinct therapeutic benefit with delayed tumor recurrence and longer survival. Cycling treatments with drugs and/or radiation are common procedure and often show clinical benefits. One concern regarding ABT-263 in the clinic is the thrombocytopenia that has been a predominant dose-limiting toxicity as both a monotherapy and in combination. This has been managed successfully in several recent trials, allowing for tolerated and biologically active combinations with kinase inhibitors such as Osimertinib (Bertino et al., 2021) and ruxolitinib (Harrison et al., 2019). However, neutropenia has been reported as a dose-limiting toxicity when navitoclax was administered with chemotherapy (Puglisi et al., 2011); this toxicity has been particularly limiting for these combinations, none of which have progressed beyond phase 1. Our data indicate that sequential exposures to ABT-263 after cisplatin treatment can effectively reduce tumor burden, and therefore alleviate the need to dose both agents concomitantly. This sequential dosing approach thus has the potential to effectively treat head and neck cancer patients while circumventing the limiting hematologic toxicity that would be anticipated by simultaneous dosing of the two agents. Next-generation BCL-2/BCL-X_L inhibitors, such as AZD0466 (Patterson et al., 2021), APG-1252 (Lakhani et al., 2018), and DT2216 (BCL-X_L-PROTAC) (He et al., 2020), have been designed to mitigate thrombocytopenia, and clinical trials have recently started with these agents. Thus, these compounds also need to be verified as senolytics to be combined with existing chemotherapy/targeting drugs in the future. It is also imperative to determine the senolytic efficacy following chemoradiation, which is commonly used as the first line treatment of HNSCC patients.

Taken together, our study provides a clear foundation upon which to develop therapeutic approaches for senescence clearance to potentially prevent or delay cancer relapse in HNSCC. Additionally, our in vitro and in vivo data show that sequential treatment of cisplatin and navitoclax can provide a potentially effective treatment strategy with mitigated toxicity for HNSCC patients. However, there are still key questions that need to be answered in future studies, such as the mechanistic basis for recovery from senescence, and the potential interplay between navitoclax and the immune system. Furthermore, studies in progress suggest that navitoclax may not be effective in cisplatin-resistant head and neck cancer models; consequently, we are in the process of identifying alternative senolytic strategies for eliminating the resistant population as well as testing senolytics against chemoradiation, the standard of care in head and neck cancer.

Acknowledgments

Tissue sectioning was provided by the VCU Tissue and Data Acquisition and Analysis Core (TDAAC) Facility. All flow cytometry data were generated at the VCU Massey Cancer Center Flow Cytometry Shared Resource.

Authorship Contributions

Participated in research design: Ahmadinejad, Gewirtz, Harada.

Conducted experiments: Ahmadinejad, Bos, Hu, Britt.

Contributed new reagents or analytic tools: Koblinski, Souers, Leverson, Faber.

Performed data analysis: Ahmadinejad, Bos, Gewirtz, Harada.

Wrote or contributed to the writing of the manuscript: Ahmadinejad, Bos, Souers, Gewirtz, Harada.

References

Alotaibi M, Sharma K, Saleh T, Povirk LF, Hendrickson EA, and Gewirtz DA (2016) Radiosensitization by PARP inhibition in DNA repair proficient and deficient tumor cells: proliferative recovery in senescent cells. *Radiat Res* **185**:229–245.

Ang KK, Zhang Q, Rosenthal DI, Nguyen-Tan PF, Sherman EJ, Weber RS, Galvin JM, Bonner JA, Harris J, El-Naggar AK, et al. (2014) Randomized phase III trial of concurrent accelerated radiation plus cisplatin with or without cetuximab for stage III to IV head and neck carcinoma: RTOG 0522. *J Clin Oncol* **32**:2940–2950.

Argiris A, Karamouzis MV, Raben D, and Ferris RL (2008) Head and neck cancer. *Lancet* **371**:1695–1709.

Baker DJ, Wijshake T, Tchkonia T, LeBrasseur NK, Childs BG, van de Sluis B, Kirkland JL, and van Deursen JM (2011) Clearance of p16Ink4a-positive senescent cells delays ageing-associated disorders. *Nature* **479**:232–236.

Basu A and Krishnamurthy S (2010) Cellular responses to cisplatin-induced DNA damage. *J Nucleic Acids* **2010**:1–16.

Beauséjour CM, Krtolica A, Galimi F, Narita M, Lowe SW, Yaswen P, and Campisi J (2003) Reversal of human cellular senescence: roles of the p53 and p16 pathways. *EMBO J* **22**:4212–4222.

Bertino EM, Gentzler RD, Clifford S, Kolesar J, Muzikansky A, Haura EB, Piotrowska Z, Camidge DR, Stinchcombe TE, Hann C, et al. (2021) Phase IB study of osimertinib in combination with navitoclax in *EGFR*-mutant NSCLC following resistance to initial *EGFR* therapy (ETCTN 9903). *Clin Cancer Res* **27**:1604–1611.

Carpenter V, Saleh T, Min Lee S, Murray G, Reed J, Souers A, Faber AC, Harada H, and Gewirtz DA (2021) Androgen-deprivation induced senescence in prostate cancer cells is permissive for the development of castration-resistance but susceptible to senolytic therapy. *Biochem Pharmacol* **193**:114765.

Carter RJ, Milani M, Butterworth M, Alotibi A, Harper N, Yedida G, Greaves G, Al-Zebeeby A, Jorgensen AL, Schache AG, et al. (2019) Exploring the potential of BH3 mimetic therapy in squamous cell carcinoma of the head and neck. *Cell Death Dis* **10**:912.

Chen J, Jin S, Abraham V, Huang X, Liu B, Mitten MJ, Nimmer P, Lin X, Smith M, Shen Y, et al. (2011) The Bcl-2/Bcl-X($_L$)/Bcl-w inhibitor, navitoclax, enhances the activity of chemotherapeutic agents *in vitro* and *in vivo*. *Mol Cancer Ther* **10**:2340–2349.

Chitikova ZV, Gordeev SA, Bykova TV, Zubova SG, Pospelov VA, and Pospelova TV (2014) Sustained activation of DNA damage response in irradiated apoptosis-resistant cells induces reversible senescence associated with mTOR downregulation and expression of stem cell markers. *Cell Cycle* **13**:1424–1439.

Chow LQM (2020) Head and Neck Cancer. *N Engl J Med* **382**:60–72.

Coppé J-P, Desprez P-Y, Krtolica A, and Campisi J (2010) The senescence-associated secretory phenotype: the dark side of tumor suppression. *Annu Rev Pathol* **5**:99–118.

Cramer JD, Burtness B, Le QT, and Ferris RL (2019) The changing therapeutic landscape of head and neck cancer. *Nat Rev Clin Oncol* **16**:669–683.

Debacq-Chainiaux F, Erusalimsky JD, Campisi J, and Toussaint O (2009) Protocols to detect senescence-associated beta-galactosidase (SA-betagal) activity, a biomarker of senescent cells in culture and in vivo. *Nat Protoc* **4**:1798–1806.

Demaria M, O'Leary MN, Chang J, Shao L, Liu S, Alimirah F, Koenig K, Le C, Mitin N, Deal AM, et al. (2017) Cellular Senescence Promotes Adverse Effects of Chemotherapy and Cancer Relapse. *Cancer Discov* **7**:165–176.

Dimri GP, Lee X, Basile G, Acosta M, Scott G, Roskelley C, Medrano EE, Linskens M, Rubelj I, Pereira-Smith O, et al. (1995) A biomarker that identifies senescent human cells in culture and in aging skin in vivo. *Proc Natl Acad Sci USA* **92**:9363–9367.

Dirac AMG and Bernards R (2003) Reversal of senescence in mouse fibroblasts through lentiviral suppression of p53. *J Biol Chem* **278**:11731–11734.

Donà MG, Rollo F, Pichi B, Spriano G, Moretto S, Covello R, Pellini R, and Benevolo M (2020) Evolving profile of HPV-driven oropharyngeal squamous cell carcinoma in

a national cancer institute in Italy: A 10-year retrospective study. *Microorganisms* **8**:1498.
Duy C, Li M, Teater M, Meydan C, Garrett-Bakelman FE, Lee TC, Chin CR, Durmaz C, Kawabata KC, Dhimolea E, et al. (2021) Chemotherapy induces senescence-like resilient cells capable of initiating AML recurrence. *Cancer Discov* **11**:2159–8290.
Elmore LW, Di X, Dumur C, Holt SE, and Gewirtz DA (2005) Evasion of a single-step, chemotherapy-induced senescence in breast cancer cells: implications for treatment response. *Clin Cancer Res* **11**:2637–2643.
Ewald JA, Desotelle JA, Wilding G, and Jarrard DF (2010) Therapy-induced senescence in cancer. *J Natl Cancer Inst* **102**:1536–1546.
Farris FF, Dedrick RL, and King FG (1988) Cisplatin pharmacokinetics: applications of a physiological model. *Toxicol Lett* **43**:117–137.
Fiebig AA, Zhu W, Hollerbach C, Leber B, and Andrews DW (2006) Bcl-XL is qualitatively different from and ten times more effective than Bcl-2 when expressed in a breast cancer cell line. *BMC Cancer* **6**:213.
Gibson MK, Li Y, Murphy B, Hussain MHA, DeConti RC, Ensley J, and Forastiere AA; Eastern Cooperative Oncology Group (2005) Randomized phase III evaluation of cisplatin plus fluorouracil versus cisplatin plus paclitaxel in advanced head and neck cancer (E1395): an intergroup trial of the Eastern Cooperative Oncology Group. *J Clin Oncol* **23**:3562–3567.
Goss PE and Chambers AF (2010) Does tumour dormancy offer a therapeutic target? *Nat Rev Cancer* **10**:871–877.
Grezella C, Fernandez-Rebollo E, Franzen J, Ventura Ferreira MS, Beier F, and Wagner W (2018) Effects of senolytic drugs on human mesenchymal stromal cells. *Stem Cell Res Ther* **9**:108.
Harrison CN, Garcia JS, Mesa RA, Somervaille TC, Komrokji RS, Pemmaraju N, Jamieson C, Papadantonakis N, Foran JM, O'Connell CL, et al. (2019) Results from a Phase 2 Study of Navitoclax in Combination with Ruxolitinib in Patients with Primary or Secondary Myelofibrosis. *Blood* **134(Suppl)**:671.
Hayward RL, Macpherson JS, Cummings J, Monia BP, Smyth JF, and Jodrell DI (2003) Antisense Bcl-xl down-regulation switches the response to topoisomerase I inhibition from senescence to apoptosis in colorectal cancer cells, enhancing global cytotoxicity. *Clin Cancer Res* **9**:2856–2865.
He Y, Koch R, Budamagunta V, Zhang P, Zhang X, Khan S, Thummuri D, Ortiz YT, Zhang X, Lv D, et al. (2020) DT2216-a Bcl-xL-specific degrader is highly active against Bcl-xL-dependent T cell lymphomas. *J Hematol Oncol* **13**:95.
Hernandez-Segura A, de Jong TV, Melov S, Guryev V, Campisi J, and Demaria M (2017) Unmasking Transcriptional Heterogeneity in Senescent Cells. *Curr Biol* **27**:2652–2660.e4.
Hernandez-Segura A, Nehme J, and Demaria M (2018) Hallmarks of Cellular Senescence. *Trends Cell Biol* **28**:436–453.
Jeon JH, Kim SK, Kim HJ, Chang J, Ahn CM, and Chang YS (2008) Insulin-like growth factor-1 attenuates cisplatin-induced gammaH2AX formation and DNA double-strand breaks repair pathway in non-small cell lung cancer. *Cancer Lett* **272**:232–241.
Kareva I (2016) Escape from tumor dormancy and time to angiogenic switch as mitigated by tumor-induced stimulation of stroma. *J Theor Biol* **395**:11–22.
Kim RS, Avivar-Valderas A, Estrada Y, Bragado P, Sosa MS, Aguirre-Ghiso JA, and Segall JE (2012) Dormancy signatures and metastasis in estrogen receptor positive and negative breast cancer. *PLoS One* **7**:e35569.
Krizhanovsky V, Yon M, Dickins RA, Hearn S, Simon J, Miething C, Yee H, Zender L, and Lowe SW (2008) Senescence of activated stellate cells limits liver fibrosis. *Cell* **134**:657–667.
Lafontaine J, Cardin GB, Malaquin N, Boisvert J-S, Rodier F, and Wong P (2021) Senolytic targeting of Bcl-2 anti-apoptotic family increases cell death in irradiated sarcoma cells. *Cancers (Basel)* **13**:386.
Lakhani NJ, Rasco DW, Tolcher AW, Huang Y, Ji J, Wang H, Dong Q, Men L, O'Rourke TJ, Chandana SR, et al. (2018) A phase I study of novel dual Bcl-2/Bcl-xL inhibitor APG-1252 in patients with advanced small cell lung cancer (SCLC) or other solid tumor. *J Clin Oncol* **36(Suppl)**:2594.
Lambrecht M, Dirix P, Van den Bogaert W, and Nuyts S (2009) Incidence of isolated regional recurrence after definitive (chemo-) radiotherapy for head and neck squamous cell carcinoma. *Radiother Oncol* **93**:498–502.
Leemans CR, Braakhuis BJM, and Brakenhoff RH (2011) The molecular biology of head and neck cancer. *Nat Rev Cancer* **11**:9–22.
Mas-Bargues C, Borrás C, and Viña J (2021) Bcl-xL as a Modulator of Senescence and Aging. *Int J Mol Sci* **22**:1527.
Mérino D, Khaw SL, Glaser SP, Anderson DJ, Belmont LD, Wong C, Yue P, Robati M, Phipson B, Fairlie WD, et al. (2012) Bcl-2, Bcl-x(L), and Bcl-w are not equivalent targets of ABT-737 and navitoclax (ABT-263) in lymphoid and leukemic cells. *Blood* **119**:5807–5816.
Mirzayans R, Andrais B, Hansen G, and Murray D (2012) Role of p16(INK4A) in replicative senescence and DNA damage-induced premature senescence in p53-deficient human cells. *Biochem Res Int* **2012**:1–8.
Morgan TM, Lange PH, Porter MP, Lin DW, Ellis WJ, Gallaher IS, and Vessella RL (2009) Disseminated tumor cells in prostate cancer patients after radical prostatectomy and without evidence of disease predicts biochemical recurrence. *Clin Cancer Res* **15**:677–683.
Nardella C, Clohessy JG, Alimonti A, and Pandolfi PP (2011) Pro-senescence therapy for cancer treatment. *Nat Rev Cancer* **11**:503–511.
Oltersdorf T, Elmore SW, Shoemaker AR, Armstrong RC, Augeri DJ, Belli BA, Bruncko M, Deckwerth TL, Dinges J, Hajduk PJ, et al. (2005) An inhibitor of Bcl-2 family proteins induces regression of solid tumours. *Nature* **435**:677–681.
Patterson CM, Balachander SB, Grant I, Pop-Damkov P, Kelly B, McCoull W, Parker J, Giannis M, Hill KJ, Gibbons FD, et al. (2021) Design and optimisation of dendrimer-conjugated Bcl-2/x_L inhibitor, AZD0466, with improved therapeutic index for cancer therapy. *Commun Biol* **4**:112.
Pena JC, Thompson CB, Recant W, Vokes EE, and Rudin CM (1999) Bcl-xL and Bcl-2 expression in squamous cell carcinoma of the head and neck. *Cancer* **85**:164–170.
Pérez-Mancera PA, Young ARJ, and Narita M (2014) Inside and out: the activities of senescence in cancer. *Nat Rev Cancer* **14**:547–558.
Phi LTH, Sari IN, Yang Y-G, Lee S-H, Jun N, Kim KS, Lee YK, and Kwon HY (2018) Cancer stem cells (CSCs) in drug resistance and their therapeutic implications in cancer treatment. *Stem Cells Int* **2018**:1–16.
Puglisi M, Molife LR, de Jonge MJ, Khan KH, Doorn LV, Forster MD, Blanco M, Gutierrez M, Franklin C, Busman T, et al. (2021) A Phase I study of the safety, pharmacokinetics and efficacy of navitoclax plus docetaxel in patients with advanced solid tumors. *Future Oncol* **17**:2747–2758.
Puglisi M, van Doorn L, Blanco-Codesido M, De Jonge MJ, Moran K, Yang J, Busman T, Franklin C, Mabry M, Krivoshik A, et al. (2011) A phase I safety and pharmacokinetic (PK) study of navitoclax (N) in combination with docetaxel (D) in patients (pts) with solid tumors. *J Clin Oncol* **29(Suppl)**:2518.
Puig P-E, Guilly M-N, Bouchot A, Droin N, Cathelin D, Bouyer F, Favier L, Ghiringhelli F, Kroemer G, Solary E, et al. (2008) Tumor cells can escape DNA-damaging cisplatin through DNA endoreduplication and reversible polyploidy. *Cell Biol Int* **32**:1031–1043.
Raffo AJ, Perlman H, Chen MW, Day ML, Streitman JS, and Buttyan R (1995) Overexpression of bcl-2 protects prostate cancer cells from apoptosis in vitro and confers resistance to androgen depletion in vivo. *Cancer Res* **55**:4438–4445.
Rebbaa A (2005) Targeting senescence pathways to reverse drug resistance in cancer. *Cancer Lett* **219**:1–13.
Renault TT, Teijido O, Missire F, Ganesan YT, Velours G, Arokium H, Beaumatin F, Llanos R, Athané A, Camougrand N, et al. (2015) Bcl-xL stimulates Bax relocation to mitochondria and primes cells to ABT-737. *Int J Biochem Cell Biol* **64**:136–146.
Rezaee M, Sanche L, and Hunting DJ (2013) Cisplatin enhances the formation of DNA single- and double-strand breaks by hydrated electrons and hydroxyl radicals. *Radiat Res* **179**:323–331.
Roberson RS, Kussick SJ, Vallieres E, Chen S-YJ, and Wu DY (2005) Escape from therapy-induced accelerated cellular senescence in p53-null lung cancer cells and in human lung cancers. *Cancer Res* **65**:2795–2803.
Roberts AW, Wilson W, Gandhi L, O'Connor OA, Rudin CM, Brown JR, Xiong H, Chiu Y, Enschede S, and Krivoshik AP (2009) Ongoing phase I studies of ABT-263: Mitigating Bcl-X_L induced thrombocytopenia with lead-in and continuous dosing. *J Clin Oncol* **27(Suppl)**:3505.
Rudin CM, Hann CL, Garon EB, Ribeiro de Oliveira M, Bonomi PD, Camidge DR, Chu Q, Giaccone G, Khaira D, Ramalingam SS, et al. (2012) Phase II study of single-agent navitoclax (ABT-263) and biomarker correlates in patients with relapsed small cell lung cancer. *Clin Cancer Res* **18**:3163–3169.
Saleh T, Bloukh S, Carpenter VJ, Alwohoush E, Bakeer J, Darwish S, Azab B, and Gewirtz DA (2020a) Therapy-Induced Senescence: An "Old" Friend Becomes the Enemy. *Cancers (Basel)* **12**:822.
Saleh T, Carpenter VJ, Tyutyunyk-Massey L, Murray G, Leverson JD, Souers AJ, Alotaibi MR, Faber AC, Reed J, Harada H, et al. (2020b) Clearance of therapy-induced senescent tumor cells by the senolytic ABT-263 via interference with BCL-X_L -BAX interaction. *Mol Oncol* **14**:2504–2519.
Saleh T, Tyutyunyk-Massey L, Murray GF, Alotaibi MR, Kawale AS, Elsayed Z, Henderson SC, Yakovlev V, Elmore LW, Toor A, et al. (2019) Tumor cell escape from therapy-induced senescence. *Biochem Pharmacol* **162**:202–212.
Seluanov A, Gorbunova V, Falcovitz A, Sigal A, Milyavsky M, Zurer I, Shohat G, Goldfinger N, and Rotter V (2001) Change of the death pathway in senescent human fibroblasts in response to DNA damage is caused by an inability to stabilize p53. *Mol Cell Biol* **21**:1552–1564.
Sharma K, Goehe RW, Di X, Hicks 2nd MA, Torti SV, Torti FM, Harada H, and Gewirtz DA (2014) A novel cytostatic form of autophagy in sensitization of non-small cell lung cancer cells to radiation by vitamin D and the vitamin D analog, EB 1089. *Autophagy* **10**:2346–2361.
Sharpless NE and Sherr CJ (2015) Forging a signature of in vivo senescence. *Nat Rev Cancer* **15**:397–408.
Shay JW and Roninson IB (2004) Hallmarks of senescence in carcinogenesis and cancer therapy. *Oncogene* **23**:2919–2933.
Shoemaker AR, Mitten MJ, Adickes J, Oleksijew A, Zhang H, Bauch J, Marsh K, Frost DJ, Madar D, Tse C, et al. (2006) The Bcl-2 family inhibitor ABT-263 shows significant but reversible thrombocytopenia in mice. *Blood* **108**:1107.
Sieben CJ, Sturmlechner I, van de Sluis B, and van Deursen JM (2018) Two-step senescence-focused cancer therapies. *Trends Cell Biol* **28**:723–737.
Singchat W, Hitakomate E, Rerkarmnuaychoke B, Suntronpong A, Fu B, Bodhisuwan W, Peyachoknagul S, Yang F, Koontongkaew S, and Srikulnath K (2016) Genomic alteration in head and neck squamous cell carcinoma (HNSCC) cell lines inferred from karyotyping, molecular cytogenetics, and array comparative genomic hybridization. *PLoS One* **11**:e0160901.
Sosa MS, Bragado P, and Aguirre-Ghiso JA (2014) Mechanisms of disseminated cancer cell dormancy: an awakening field. *Nat Rev Cancer* **14**:611–622.
Triana-Martínez F, Loza MI, and Domínguez E (2020) Beyond tumor suppression: Senescence in cancer stemness and tumor dormancy. *Cells* **9**:346.
Tse C, Shoemaker AR, Adickes J, Anderson MG, Chen J, Jin S, Johnson EF, Marsh KC, Mitten MJ, Nimmer P, et al. (2008) ABT-263: a potent and orally bioavailable Bcl-2 family inhibitor. *Cancer Res* **68**:3421–3428.
Urien S and Lokiec F (2004) Population pharmacokinetics of total and unbound plasma cisplatin in adult patients. *Br J Clin Pharmacol* **57**:756–763.
Walens A, DiMarco AV, Lupo R, Kroger BR, Damrauer JS, and Alvarez JV (2019) CCL5 promotes breast cancer recurrence through macrophage recruitment in residual tumors. *eLife* **8**:e43653.
Wang H, Stoecklein NH, Lin PP, and Gires O (2017) Circulating and disseminated tumor cells: diagnostic tools and therapeutic targets in motion. *Oncotarget* **8**:1884–1912.

Wang Q, Wu PC, Dong DZ, Ivanova I, Chu E, Zeliadt S, Vesselle H, and Wu DY (2013) Polyploidy road to therapy-induced cellular senescence and escape. *Int J Cancer* **132**:1505–1515.

Wang X, Zhang J, Kim HP, Wang Y, Choi AMK, and Ryter SW (2004) Bcl-X_L disrupts death-inducing signal complex formation in plasma membrane induced by hypoxia/reoxygenation. *FASEB J* **18**:1826–1833.

Wiley CD, Flynn JM, Morrissey C, Lebofsky R, Shuga J, Dong X, Unger MA, Vijg J, Melov S, and Campisi J (2017) Analysis of individual cells identifies cell-to-cell variability following induction of cellular senescence. *Aging Cell* **16**:1043–1050.

Wu C-Y, Lee C-L, Wu C-F, Fu J-Y, Yang C-T, Wen C-T, Liu Y-H, Liu H-P, and Hsieh JC-H (2020) Circulating tumor cells as a tool of minimal residual disease can predict lung cancer recurrence: A longitudinal, prospective trial. *Diagnostics (Basel)* **10**:144.

Yabluchanskiy A, Tarantini S, Balasubramanian P, Kiss T, Csipo T, Fülöp GA, Lipecz A, Ahire C, DelFavero J, Nyul-Toth A, et al. (2020) Pharmacological or genetic depletion of senescent astrocytes prevents whole brain irradiation-induced impairment of neurovascular coupling responses protecting cognitive function in mice. *Geroscience* **42**:409–428.

Yang L, Fang J, and Chen J (2017) Tumor cell senescence response produces aggressive variants. *Cell Death Discov* **3**:17049.

Yeh AC and Ramaswamy S (2015) Mechanisms of cancer cell dormancy—another hallmark of cancer? *Cancer Res* **75**:5014–5022.

Yosef R, Pilpel N, Tokarsky-Amiel R, Biran A, Ovadya Y, Cohen S, Vadai E, Dassa L, Shahar E, Condiotti R, et al. (2016) Directed elimination of senescent cells by inhibition of BCL-W and BCL-XL. *Nat Commun* **7**:11190.

Zhu Y, Tchkonia T, Fuhrmann-Stroissnigg H, Dai HM, Ling YY, Stout MB, Pirtskhalava T, Giorgadze N, Johnson KO, Giles CB, et al. (2016) Identification of a novel senolytic agent, navitoclax, targeting the Bcl-2 family of anti-apoptotic factors. *Aging Cell* **15**:428–435.

Zhu Y, Tchkonia T, Pirtskhalava T, Gower AC, Ding H, Giorgadze N, Palmer AK, Ikeno Y, Hubbard GB, Lenburg M, et al. (2015) The Achilles' heel of senescent cells: from transcriptome to senolytic drugs. *Aging Cell* **14**:644–658.

Address correspondence to: Hisashi Harada, Virginia Commonwealth University, 401 College Street, Richmond, VA 23298. E-mail: hharada@vcu.edu; or David A. Gewirtz, Virginia Commonwealth University, 401 College Street, Richmond, VA 23298. E-mail: david.gewirtz@vcuhealth.org

Supplementary Data*:*

Senolytic-mediated elimination of head and neck tumor cells induced into senescence by cisplatin

Fereshteh Ahmadinejad[1*], Tasia Bos[2*], Bin Hu[3], Erin Britt[2], Jennifer Koblinski[3], Andrew J. Souers[4], Joel D. Leverson[4], Anthony C. Faber[2], David A. Gewirtz[5#], Hisashi Harada[2#]

1: Department of Human and Molecular Genetics, School of Medicine, Massey Cancer Center, Virginia Commonwealth University, Richmond, Virginia

2: Philips Institute for Oral Health Research, School of Dentistry, Massey Cancer Center, Virginia Commonwealth University, Richmond, Virginia

3: Cancer Mouse Models Core, Massey Cancer Center, Virginia Commonwealth University, Richmond, Virginia

4: AbbVie, North Chicago, Illinois

5: Department of Pharmacology and Toxicology, School of Medicine, Massey Cancer Center, Virginia Commonwealth University, Richmond, Virginia

Figure S1

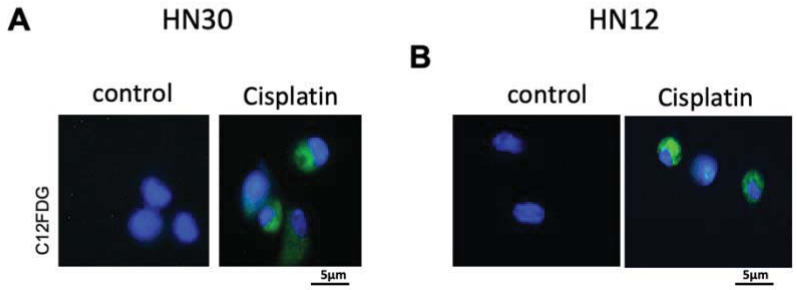

Figure S1. Immunofluorescence imaging of C_{12}FDG in **A)** HN30 and **B)** HN12 cells after senescence induction by 5 µM cisplatin. Blue fluorescence indicates nuclear staining with DAPI, and green fluorescence reflects C12FDG immunostaining.

Figure S2

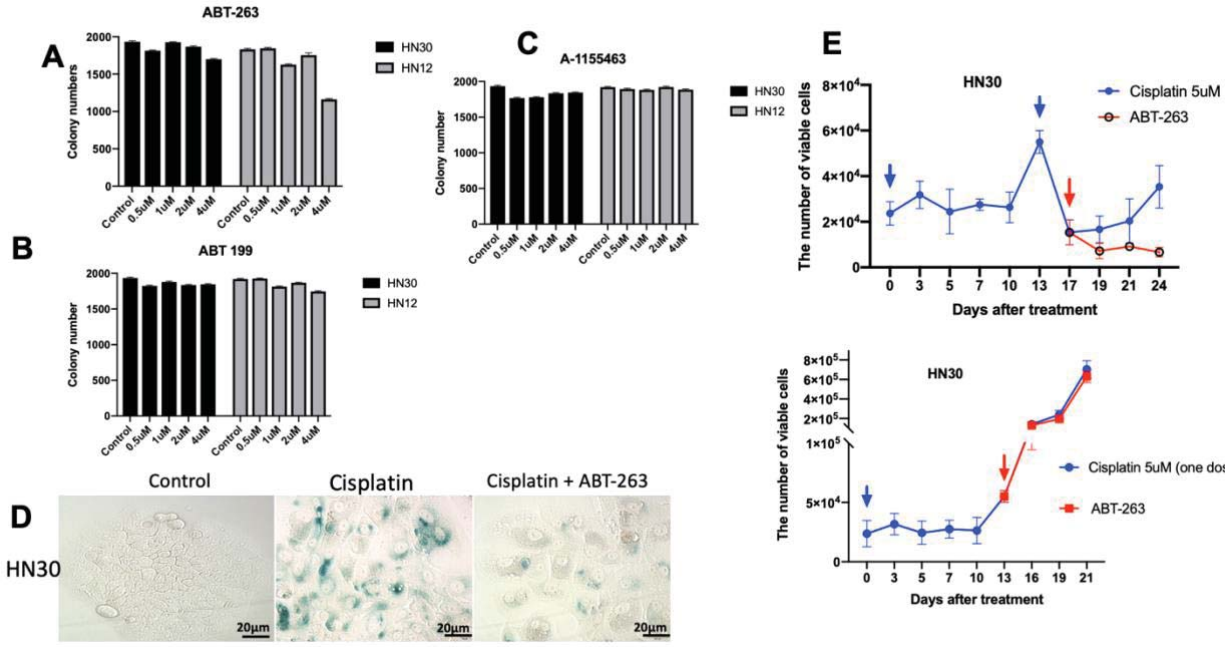

Figure S2. ABT-263 has minimal cytotoxicity on non-senescent cells or proliferative recovering cells from senescence. A, B, and C) Clonogenic survival assay performed on control cells treated with different concentrations of ABT-263 for 24 hours. The number of colonies were counted and analyzed. **D)** X-gal staining after sequential treatment of HN30 cells with cisplatin and ABT-263; decreased population of SA-β-gal positive cells show that ABT-263 treatment eliminates senescent cells**. E)** ABT-263 effectiveness diminishes over time when HN30 cells recover their proliferative capacity. Blue arrows indicate the cisplatin treatment timepoint. Red arrows are ABT-263 treatment timepoints. Note that HN30 cells undergo cell death only when they are in senescence state (top), but not in recovery stage (bottom). All quantitative graphs are mean ± SD from at least three independent experiments.

Figure S3

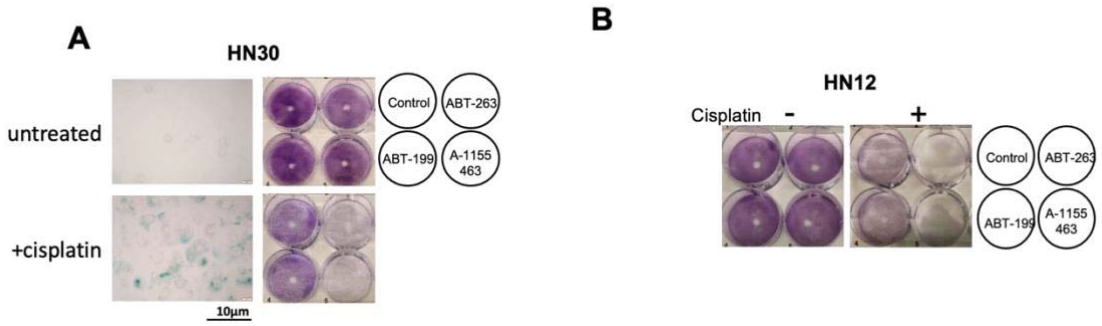

Figure S3. BCL-X_L is the primary target for ABT-263-induced senolysis. Clonogenic survival assay performed on **A)** HN30 **and B)** HN12 cells treated with vehicle or cisplatin followed by ABT-263, ABT-199, and A-1155463 (1uM for 24 hours).

Figure S4

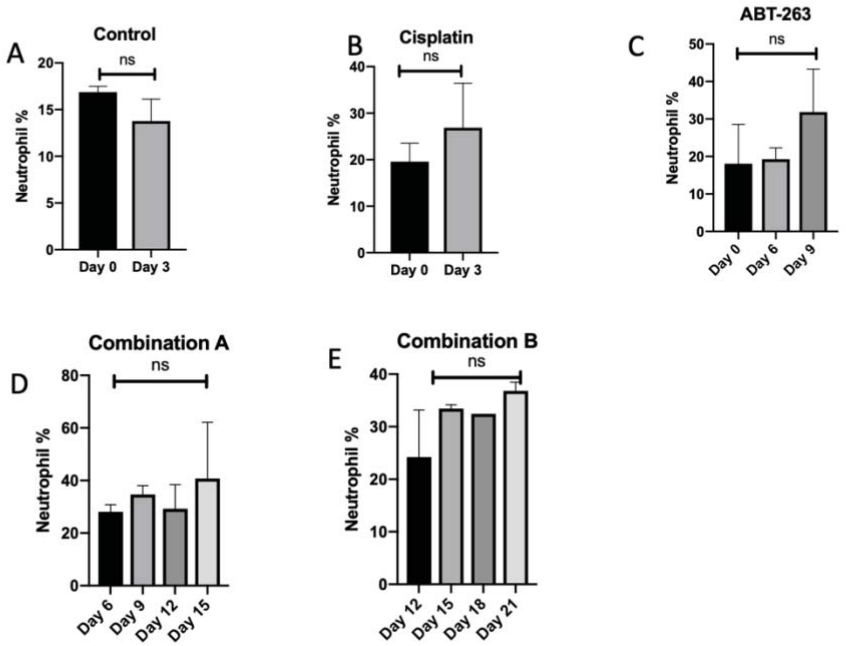

Figure S4. Cisplatin, ABT-263 treatment alone or in combination did not result in significant Neutropenia. Blood samples were analyzed for neutrophil percentage at different time points in different groups of **A)** control, **B)** Cisplatin alone, **C)** ABT-263, **D** and **E)** cisplatin in combination with ABT-263. Control vs ABT, cisplatin, Combination A or B: $p > 0.05$ All quantitative graphs are mean ± SD from at least three independent experiments. * $p \leq 0.05$, ** $p \leq 0.01$, *** $p \leq 0.001$, **** $p \leq 0.0001$ 0001 indicate statistical significance of each condition compared to indicated condition as determined using two ‑ way ANOVA with Sidak's post hoc test.

Figure S5

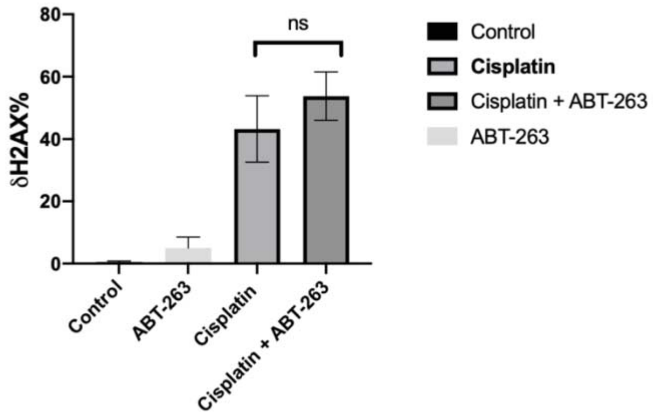

Figure S5. Cisplatin, ABT-263 treatment alone or in combination did not result in significant levels of DNA double strand breaks measured by γ-H2AX levels. $p > 0.05$ All quantitative graphs are mean ± SD from at least three independent experiments. * $p \leq 0.05$, ** $p \leq 0.01$, *** $p \leq 0.001$, **** $p \leq 0.0001$ 0001 indicate statistical significance of each condition compared to indicated condition as determined using two‐way ANOVA with Sidak's post hoc test.

Figure S6

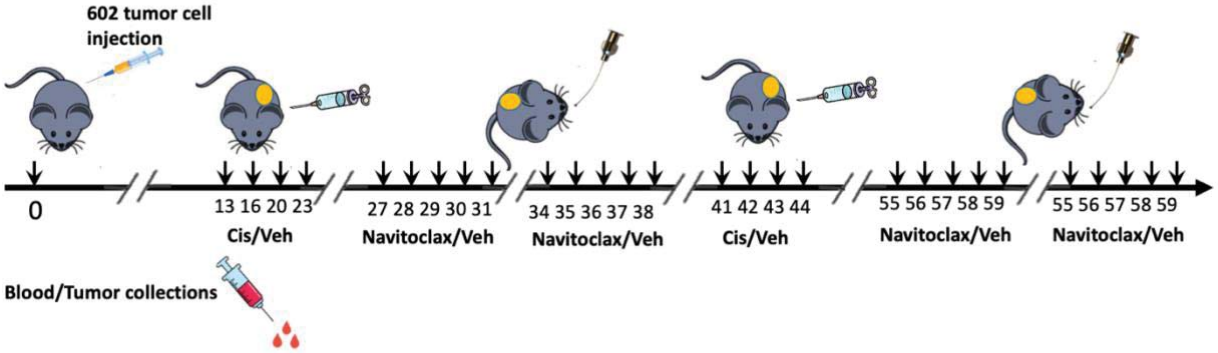

Figure S6. Animal experiments diagram.